AMERICAN UNIVERSITY OF BEIRUT

OPTIMAL DESIGN OF AN ADVANCED FUEL CELL HYBRID ELECTRIC VEHICLE

by
CHAYBAN MIKHAEL GHABECH

A thesis
submitted in partial fulfillment of the requirements
for the degree of Master of Engineering
to the Department of Electrical and Computer Engineering
of the Faculty of Engineering and Architecture
at the American University of Beirut

Beirut, Lebanon
July 2019

AMERICAN UNIVERSITY OF BEIRUT

OPTIMAL DESIGN OF AN ADVANCED FUEL CELL HYBRID
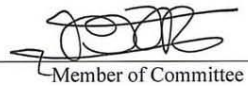ELECTRIC VEHICLE

by

CHAYBAN MIKHAEL GHABECH

Approved by:

_____
Prof. Sami Karaki, Chairperson   Advisor
Electrical and Computer Engineering

_____
Prof. Ali Bazzi, Associate Professor   Co-Advisor
Electrical and Computer Engineering

_____
Prof. Rabih Jabr, Professor   Member of Committee
Electrical and Computer Engineering

_____
Prof. Vida Mia Garcia, Professor   Member of Committee
Stanford University

Date of thesis defense: July 18, 2019

AMERICAN UNIVERSITY OF BEIRUT

THESIS, DISSERTATION, PROJECT RELEASE FORM

Student Name: _Cohobech_ _Chayboun_ _Mikhael_
                 Last   First   Middle

☑ Master's Thesis   ◯ Master's Project   ◯ Doctoral Dissertation

☐   I authorize the American University of Beirut to: (a) reproduce hard or electronic copies of my thesis, dissertation, or project; (b) include such copies in the archives and digital repositories of the University; and (c) make freely available such copies to third parties for research or educational purposes.

☑   I authorize the American University of Beirut, to: (a) reproduce hard or electronic copies of it; (b) include such copies in the archives and digital repositories of the University; and (c) make freely available such copies to third parties for research or educational purposes after:

         One ---- year from the date of submission of my thesis, dissertation, or
project.
         Two ---- years from the date of submission of my thesis, dissertation, or
project.
         Three ✓--- years from the date of submission of my thesis, dissertation, or
project.

CCe   _August, 2, 2019_

Signature   Date

ACKNOWLEDGMENTS

AN ABSTRACT OF THE THESIS OF

Chayban Mikhael Ghabech   for   Master of Engineering

                                    Major: Electrical and Computer Engineering

Title: Optimal design of an advanced fuel cell hybrid electric vehicle

The optimal sizing of the fuel cell, battery, motor and hydrogen tank of a fuel cell hybrid electric vehicle (FCHEV) is achieved using a search tool based on Ordinal Optimization (OO). It incorporates a FCHEV optimal simulation tool that uses an approximate version of dynamic programming known as Single Stage Dynamic Programming (SSDP). The SSDP method is further enhanced as a Two-Step SSDP to reduce the operation simulation time to about one-fourth.

In this work the effect of using light material on the power demand as well as on the hydrogen consumption will be studied and evaluated. For this purpose two separate FCHEV designs are proposed and evaluated. The first FCHEV will be a baseline model inspired from a Toyota Venza (2009) where the body of the FCHEV is mainly composed of steel/iron. The other will be an advanced model which is based on a light body vehicle inspired from a Lotus Engineering design. The suggested design will be further refined by accounting for the power losses in the electric power train. These losses will include stator and rotor copper losses in the induction motor as well as the switching and conduction losses in the inverter of the FCHEV.

In the last part of the thesis an environmental cost will be calculated for the two FCHEV designs. This cost will take into consideration the electricity generation mix used to charge the battery, and the method used to produce the hydrogen used as the fuel for PEM fuel cell. This environmental cost will be calculated if the same design is used in different regions in the world. Therefore, this thesis will not only provide an advanced FCHEV design tool, but also a technical report that can be placed in the hands of government officials and decision makers willing to integrate FCHEV into their transportation sector.

In this work we will test and simulate our FCHEV on a combination of two driving cycles consisting of the HWFET and the UDDS. In addition, proprietary acceleration and gradeability cycles are to select sizes for the motor and inverter. Our suggested design will be tested under different operating conditions such as charge sustaining and charge depletion strategies.

CONTENTS

ILLUSTRATIONS

TABLES

CHAPTER I

INTRODUCTION

A. Motivation and Objectives

Saving the environment, reducing pollution, preserving our natural resources are all great objectives but their achievements requires radical changes in energy consumption behavior. Climate change has become a major threat to earth and all its inhabitants. In fact, the World Health Organization (WHO) [1] states that climate change will cause an additional 250,000 death per year. Moreover, the WHO estimates the direct monetary cost to health to reach $4 billion per year. In fact, climate change and air pollution go hand by hand and their negative effects are long lasting. Air pollution can be defined as the presence of harmful substances in the atmosphere that damage human health and cause harmful effects on the environment. There is no doubt that the transportation sector is a great contributor of harmful pollutants into the atmosphere, which has a negative effect on our environment and our own well-being.

According to the environmental protection agency the transportation sector has the largest second share in terms of harmful emissions. This share represents 28.5 % of the total greenhouse gas emissions [2]. In fact, car exhausts make up the main ingredients of air pollution. These include: Carbon Monoxide (CO), Nitrogen Oxides ($NO_{x)}$, Particulate Matter (PM), and Hydro Carbons (HC). These gases are highly toxic especially at high concentration and are all related to respiratory disorders as well as the formation of carcinogenesis. In fact, automobile idling is a major contributor in producing harmful air contaminants and is also a big waste of our natural resources [3].

   Under the pressure from different environmental protection agencies as well as scientists and activists from all around the globe, the transportation sector has been thriving to reach innovative solutions that will curb the amount of toxic emissions from the exhausts of

vehicles. In the last few years, hybrid electric vehicles (HEVs) made a comeback to the transportation sector as a promising solution to minimize emissions and help win the battle against chronic air pollution. In fact, HEVs have been widely researched and have gained great popularity from governments and decision makers as they are a key factor in minimizing air pollution that is caused by the poisonous exhausts of traditional vehicles. Indeed, HEVs role doesn't stop at reducing emissions but it goes a step further as it helps in preserving our natural resources so that our heritage and our current resources can be passed on to future generations. Unexpectedly, to many of us the idea behind HEVs dates back to the invention of the automobile itself. The main goal, however, was not really to reduce the fuel consumption but somewhat to provide higher performance levels [4]. In 1898, in Germany Dr. Ferdinand Porshe brought to life the first HEV which used an ICE to turn on the generator that supplied power to the electric motors. Few years later, many other HEVs were introduced; most notably were the first series and the first parallel hybrid electric vehicles, which were built by the French and Belgium company: "French firm Vendovelli and Priestly" and "Pieper establishments of Liège, Belgium". Initially, the purpose behind the early design of HEVs was to help using an electric source, the underdeveloped ICE of that time and to increase the driving range of vehicles. Despite their original idea and their promising advantages HEVs didn't become a breakthrough during that period because of the huge advancement in the technology of the ICE which was heavily being used after World War I. Indeed, the ICE was greatly enhanced; for example, its power and efficiency increased, and its weight was reduced. Thus, the ICE was able to deliver the performance needed independently of any secondary sources [5-7]. Other factors that lead to the disappearance of HEVs in their early start was the fact that electricity was not available to all citizens outside the major cities as well as the cheap price of gasoline at that time. In fact, the cost of early HEVs was much higher than ICE based cars due to the very large expensive batteries [8]. Moreover, the control of powertrains in HEVs wasn't an easy task due to

limited electric/electronic circuits that were available to auto makers at that time. Finally, the battery technology during the early 19 hundreds was largely underdeveloped as early batteries for HEV applications could only provide a very limited drive range with very low performance and a slow charging time that would last for hours [9].

After almost a century of their first introduction HEVs nowadays are making a strong return to the automotive market. This comeback can be attributed to many reasons such as the advancements in battery technology, power electronics as well as in electric propulsion systems. Finally, the mass production of HEVs is encouraged by the tax incentives offered by governments and the increasing will of decision and policy makers to set strict regulations in order to curb pollution levels [9]. In addition to these factors, HEVs are gaining increasing popularity over the conventional ICE based vehicles for numerous reasons. The introduction of an electric powertrain allows HEVs to have a remarkably higher mileage with fewer emissions and lower fuel consumption. Moreover, the electric powertrain allows HEVs to capture the kinetic energy and use it to recharge the battery instead of dissipating this energy in the form of heat in traditional ICE based cars [10].

B. Literature review

1. HEV Architecture

The architecture of HEVs can be classified into three categories: the series, parallel and the series parallel. Classification is based on how the HEV is connected and how the power flows from the power source to the wheels. In this work the FCHEV is based on a parallel architecture.

In the parallel configuration, the primary source supplies power directly to the wheels as can be seen in Fig. 1.1. The secondary power source can also deliver mechanical power through the converter that draws current from the battery and supplies it to the electric motor which in turn delivers the required mechanical power to the wheels. The distinctive feature of parallel HEV configuration over the series HEV is that the power coming from the fuel cell and that

coming from the battery are summed up using coupler and thus they are both able to deliver direct power simultaneously to the wheels through the transmission system [4]. The main disadvantage of parallel HEV is the more complex control mechanism than that of the series architecture [11]. Current HEVs that use the parallel configuration are: Honda, Lexus and Ford SUVs.
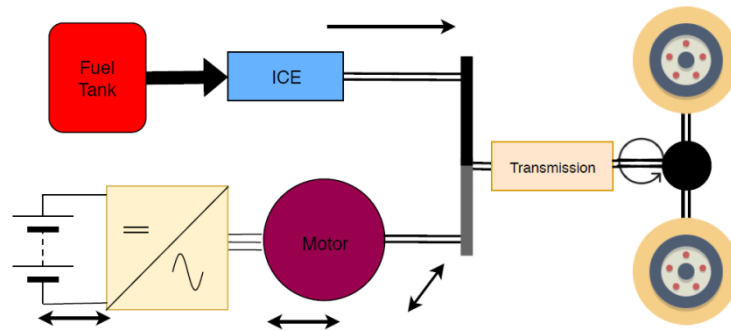
Figure 1.1 Parallel architecture of an HEV.

2. Fuel Cell versus Internal Combustion Engine

The internal combustion engine (ICE) has always been a primary powertrain in HEVs; however, fuel cells are becoming a promising source that could replace ICE in the near future. A fuel cell is an electrochemical cell which transforms chemical energy into electrical energy.

Fuel cells are divided into 6 main groups based on their operating conditions and efficiency. The PEMFC is a very promising type of fuel cell that has been extensively researched and is currently being used in variety of applications.

A FC is composed of three main parts: anode, electrolyte and the cathode as seen in Fig. 1.2.
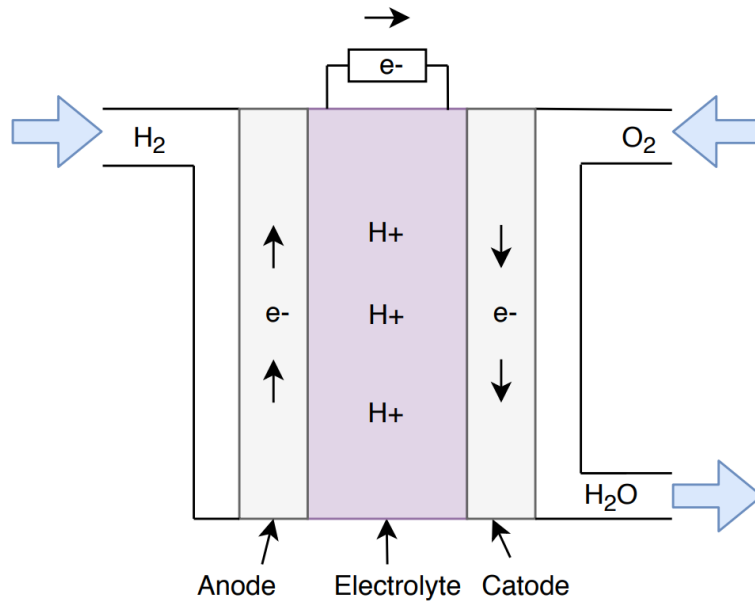
Figure 1.2 Fuel cell

The electrochemical equation of a FC is given by [12]:

$$2H_2(g) + O_2(g) \rightarrow 2H_2O + electrical\ energy + heat \qquad (1.1)$$
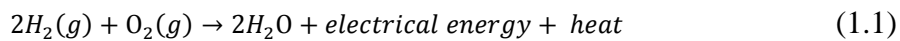
Mixing the fuel (H2) and the oxidant O2 will produce electrical energy. Heat and water are

bi-products of the process; however, zero emissions are produced. On the other hand, the fuel

combustion in an ICE releases very harmful emissions such as HC, PM, CO and NO_x. The

major difference between a FC and an ICE is that the first combines the fuel and the oxidant

in an electrochemical manner while the latter combines the fuel and the oxidant in a

combustion manner [13]. The structure of an ICE is much more complex than that of a FC. In

fact, a FC has a static structure that doesn't involve any movements of heavy mechanical

systems and it does not produce noise and does not require maintenance as the ICE does [14].

Usually the number of energy conversion from one form into another and the overall

efficiency of a system are inversely proportional. The electricity generated by a FC is the

direct product of a chemical reaction unlike the electricity that is produced by the ICE in

which chemical energy is converted to mechanical energy by combustion which is then

converted to electric energy by means of an electric generator [15]. Thus, we can conclude

that the overall efficiency of generating electricity from an FC is higher than that of an ICE.

Braga et al. [15] analyzed two systems: one that is ICE based while the other is FC based

where both systems are generating 5 kW. Braga el al. [15] report that PEMFC could replace the ICE in the near future as the results showed that the PEMFC had a 20 % higher efficiency with very low emissions. In fact, he reports that the PEMFC system had an ecological efficiency of 96 % if the hydrogen used to fuel the PEMFC is obtained from ethanol by steam reforming where ethanol is produced from sugar canes. However, from an economical point of view Braga et al. state that the investment cost in an ICE is $ 500/kW while that of an PEMFC can be anywhere between 1000 $/kW and 5000$/kW [15]. In fact, the high costs associated with fuel cells remain the major impediment against the wide adaption of this technology. However, as costs decrease, fuel cell hybrid electric vehicles (FCHEV) will have a great share in the HEV market [16].

3. Energy Storage System

The energy storage units that are being used in the FCHEVs industry are mainly batteries and in some cases ultra-capacitors (UCs). These storage units can be charged from regenerative braking and the electric grid (in the case of a Plug-in FCHEV) [17]. In fact, the efficiency and the all-electric range (AER) of a HEV rely mainly on these energy storage units [18]. Batteries usually have high energy density compared to UCs which have a low energy density; thus, batteries can carry more energy.

A battery is composed of two electrodes that are immersed in an electrolyte and are separated by a membrane. We will briefly discuss the Lithium-ion batteries (LIBs) which currently dominate the battery market and the Lead-acid batteries (LABs) which were the predecessors of LIBs.

Due to their numerous advantages Lithium-ion batteries (LIBs) are being widely used in different applications and they currently dominate the battery market. LIBs have high energy density and no battery memory [19]. In fact, an LIB has a nominal voltage of 3.6V/cell and can be operated between -20 to 60 ℃, which makes it very popular for HEV applications especially that an HEV will experience different temperatures throughout the year [20]. Due

6

to their lighter weight LIBs are becoming a popular substitute for Lead-acid batteries (LABs) especially in HEVs application where a reduction in weight increases performance and leads to additional cost savings [20]. On the other hand, LIBs suffer from numerous disadvantages. The high energy density of LIBs raises safety concerns and may threaten the life of the passengers on board [21]. Moreover, LIBs suffer from the long charging time in which an LIB needs at least two hours to be charged [22]. LIBs also have a high cost and their time is shortened by deep depth of discharge (DOD) [20]. Li et al. suggest that low cost LIBs can be achieved through minimizing scrap rate, using novel electrodes, and integrating new materials [23].

For over a century, Lead-acid batteries have been utilized in electric vehicles. In spite of its low cost and mature technology, LABs have serious drawbacks such as sulfation and increase in temperature whenever charged or discharged [24]. To stay competitive in HEVs applications, LABs must be able to accommodate fast charging as well as high current for small time intervals [25]. If these obstacles are tackled, LABs can secure their place in future HEVs as well as in other industries.

Despite of their mature technology, the design of a battery is still limited by the fact that it should deliver high specific energy and long life cycle at a competitive price. Increasing their low power density could be accomplished by increasing the battery size. However, the cost in this case will increase and the battery would lose its market competitiveness. Another issue that all batteries suffer from, regardless of their type, comes from our daily driving condition in which the energy demanded is not constant and varies according to the road. In fact, researchers have proven that a battery life cycle can significantly deteriorate if the load is not constant.

4. Energy Management System

Unlike traditional vehicles, FCHEVs utilize energy in an efficient way due to three main features: first the electric energy used from energy storing units is generated at a higher

efficiency than that coming from an ICE. Thus, the overall average efficiency of a FCHEV is higher than a regular car. Secondly, FCHEVs capture the vehicles kinetic energy instead of dissipating it as heat. Lastly, FCHEVs use energy management system to split the power demanded between the different energy sources available in the most efficient manner. In fact, the main objective of energy management system and power control strategies is to maximize the overall efficiency of FCHEVs while minimizing fuel consumption without reducing the FCHEV performance. As seen from Fig. 1.3 control strategies are divided into two classes: rule based approach and model based approach. Rule based approach is based on human know-how engineering data, and mathematical functions [26]. Rule based-approach covers deterministic as well as fuzzy based methods. On the other hand, model-based approach also known as optimization approach is based on numerical analysis and mathematical formulation where the objective is to minimize the cost function [26].
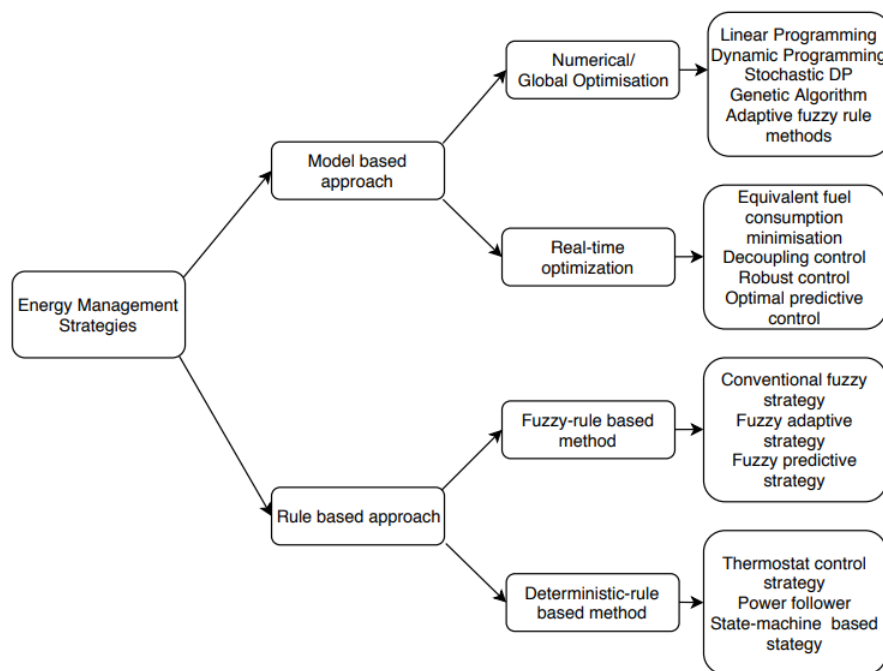
Figure 1.3 Tree diagram energy management system

Many researchers have investigated the use of rule based model strategies in FCHEVs as well as HEVs. Zhang and Tao [27] proposed a GA based fuzzy energy management system for a fuel cell/super capacitor to reduce hydrogen consumption as well as voltage and current

8

fluctuation in the fuel cell which shall prolong its lifetime. Zhang and Tao used Genetic Algorithm to select the fuzzy states and parameters of the fuzzy functions. Their proposed EMS was tested on three driving cycles HWFET UDDS NEDC. The results showed that the voltage and current fluctuations were minimized at the expense of a small short-term increase in hydrogen consumption.

Jin et al. [28] used a global optimization strategy based on DP. Upon the results of the DP the improved fuzzy controller's parameters are optimized. Jin et al [28], tested and verified their approach on two driving cycles the CYC_UDDS and US06_UDDS. On the first driving cycle the improved fuzzy controller maintained the battery SOC at 60 % throughout the whole cycle which helps maintain the battery life. In the second driving cycle, Jin et al. studied the effect of the improved suggested fuzzy controller versus a normal fuzzy controller. The HEV equipped with the improved controller consumed 5.728 L/100 km while the same HEV equipped with a normal fuzzy based controller consumed 6.127/100 km. Thus an improvement of   6.53 % was observed.

Karaki et al. [29] proposed an optimal design based on dynamic programing and ordinal optimization. The vehicle operation was simulated using DP for a set of specified components while the OO selects top good designs through a simple model and then each top design is evaluated using an accurate model. Karaki et al. tested his algorithm on the UDDS and HWFET driving cycles. Rezaei et al. [30] proposed an "equivalent consumption minimization strategy which captures energy-saving opportunities" and it is based on real-time optimization. The EMS proposed doesn't require any forecast for the HEV velocity or heavy mathematical computations. Thus, it is suitable for real-time applications. Rezai et al. [30], used a Honda civic simulation model to test their strategy on five different drive cycles. Their strategy showed a reduction in fuel consumption by an average of 7% when compared to adaptive-equivalent consumption minimization strategy and by an average 20 % when compared with a rule based control strategy.

Guo et al. [31] suggested a fast algorithm for non-linear model predictive control for HEV EMS. Guo et al. [31], proposed that by combining "Gauss pseudo spectral" method along with non-linear model predictive control, a fast algorithm that is suitable for real-time applications can be obtained. The fast algorithm was tested and verified on the UDDS and the NEDC. Guo et al. report that the suggested algorithm had a higher efficiency by an average of 3 to 4 % when compared to Euler-Model predictive control especially on the UDDS driving cycle.

CHAPTER II

FUEL CELL HYBRID ELECTRIC VEHICLE DESIGN

A.FCHEV Power Train

The diagram of a parallel FCHEV powertrain is shown in Fig. 2.1. The FCHEV is powered using a fuel cell and a battery. The fuel cell type is a polymer electrolyte membrane (PEM) and it is supplied by high pressure hydrogen from the hydrogen tank. The output of the fuel cell feeds the DC bus bar. To match the DC bus voltage, the battery is connected to the DC bus via a bidirectional DC/DC converter to and allow battery discharge whenever the power demand is positive and battery charge when the demand is negative (under regenerative braking). The fuel cell and the battery are thus connected in a parallel architecture that allows them both to supply power simultaneously whenever the power demand requires so. The three-phase induction machine (IM) has a dual purpose. Its first goal is to satisfy the torque and speed requirements of the FCHEV and is thus supplied from the DC bus through a DC to AC inverter. On the other hand, when the power demand is negative, the IM acts as a generator to capture the kinetic energy of the car and converts it to electric energy in order to charge the battery instead of dissipating it as heat. Auxiliary loads such as interior lighting, comfort control, and entertainment system demands are also being accounted for as they are connected to the DC bus. Finally, the energy management system (EMS) constantly reads the power and torque demand required by the FCHEV and allocates this power in some optimal way between the fuel cell and battery. At the same time, the EMS has to take into consideration the different constraints imposed on the fuel cell and the battery such as ramp rates and battery state of charge (SOC).
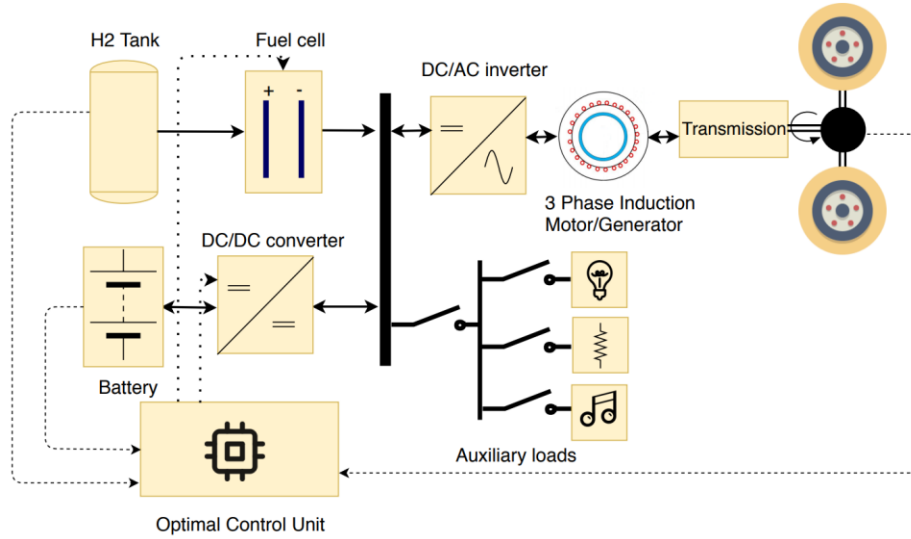
Figure 2.1 Control diagram of a parallel FCHEV

B. Problem Formulation

The problem that we are trying to solve in this work lies in finding an optimal design n for a given class of FCHEV. In other words, we must find a certain design n out of a large search space such that the annual cost function is minimized. The total annual cost function in this work is given by (2.1).

$$\hat{J} = \min_{n=1,N}(\alpha I_C(n) + O_C(n)) \qquad (2.1)$$

It has two main components: the annual investment cost and the annual operational cost denoted by $I_C(n)$ and $O_C(n)$ respectively. α is the annuity factor and $\alpha I_C(n)$ is the yearly annualized investment cost. The calculation of $I_C(n)$ is straightforward; it is equal to the given glider cost plus the cost of components used in the power train. Those components are represented by design vectors. For example, let the sampled search space be:

Fuel cell (kW) = [10, 20, 30, 40, 50, 60, 70, 80, 90, 100]
Battery (kWh) = [1, 2, 3, 4, 5, 6, 7, 8, 9, 10]
Hydrogen tank (kg) = [1, 2, 3, 4, 5, 6, 7, 8, 9, 10]
Motor (kW) = [60, 70, 80, 90, 100, 110, 120, 130, 140, 150]

The yearly operational cost is $O_C(n)$ which is defined by (2.2). $O_C(n)$ is obtained by solving for ψ once on the HWFET and once on the UDDS. By doing so, we obtain the cost function

ψ_1 and ψ_2 where these represent the operational cost function on the HWFET and on the UDDS respectively.

$$O_C(n) = M(0.45\,\psi_1(n) + 0.55\,\psi_2(n))/\,0.7 \qquad (2.2)$$

$$\psi = \min\left\{\sum_{k=1}^{K}\left[\varphi_F(F_k) + \frac{1}{2}\lambda_B B_k(sign(B_k) + 1)\right] * \Delta t\right\} \qquad (2.3)$$

ψ is the minimum operational cost function and it consists of the fuel cell cost rate plus the battery degradation cost. The fuel cell cost rate is calculated using $\varphi_F(F_k)$ which can be approximated by the quadratic polynomial (2.4).

$$\varphi_F(F_k) = a_n F_k^2 + b_n F_k + c_n \qquad (2.4)$$

The fuel cell cost curve is also plotted in Fig. 2.2. The second term in ψ stands represents the battery degradation costs. It is deduced from the Internal Battery Scaled Charged Power Map shown in Fig 2.3.
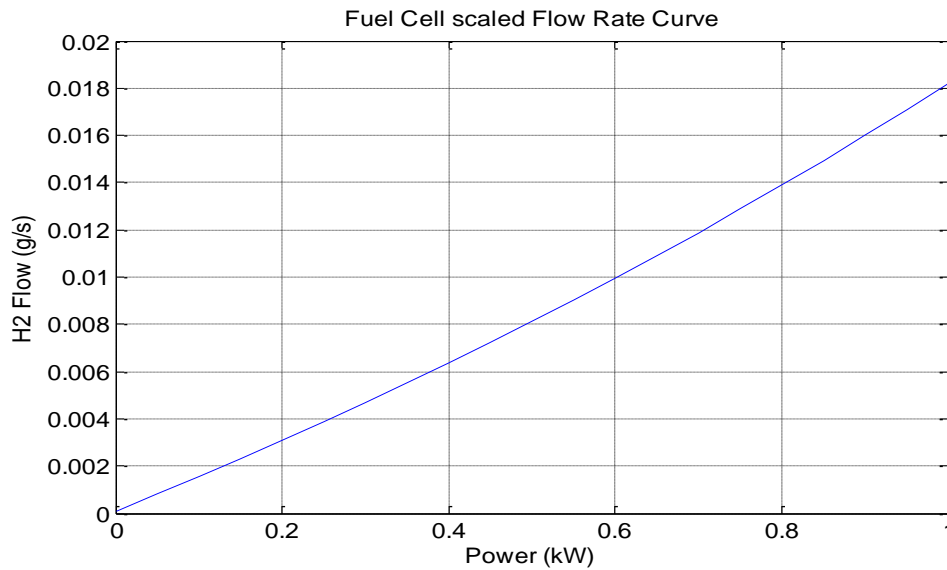
Figure 2.2 Fuel Cell Scaled Flow Rate Curve
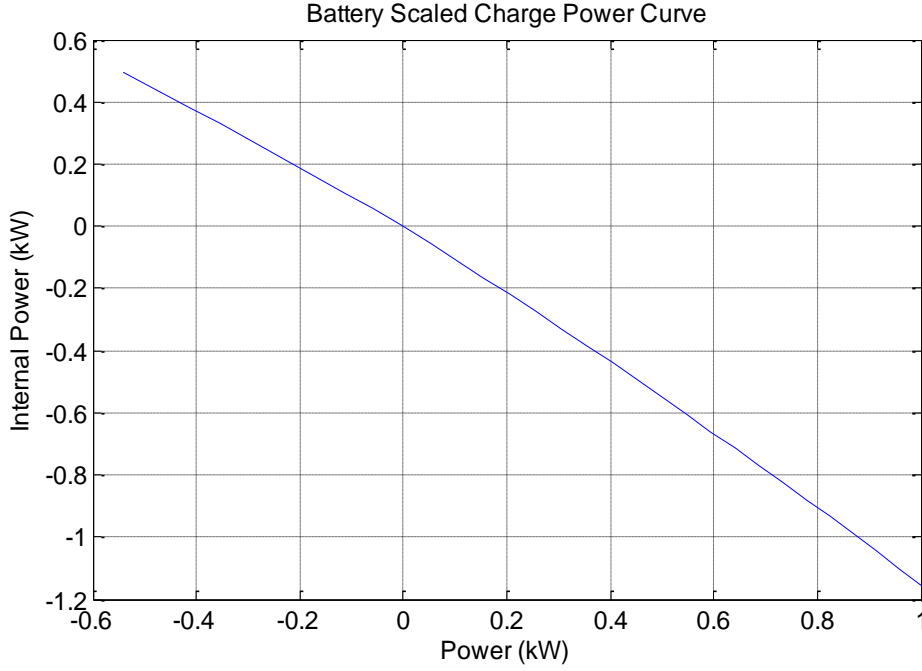
Figure 2.3 Internal Battery Scaled Charged Power Map

The EMS of a FCHEV is subject to many constraints. Most importantly an EMS should always allocate enough power supply to meet the demand. Power sources of an FCHEV are also subjected to physical constraints that bound their level of operation.

$$P_{FC}(t) + P_{BT}(t) - P_{BR}(t) = P_D(t) \tag{2.5}$$

$$P_{FC}(t)^{min} \leq P_{FC}(t) \leq P_{FC}(t)^{max} \tag{2.6}$$

$$S_{OC}(t)^{min} \leq S_{OC}(t) \leq S_{OC}(t)^{max} \tag{2.7}$$

$$-R_{dFC}\Delta T \leq P_{FC}(t) - P_{FC}(t-1) \leq R_{uFC}\Delta T \tag{2.8}$$

$$-R_{dBT}\Delta T \leq P_{BT}(t) - P_{BT}(t-1) \leq R_{uBT}\Delta T \tag{2.9}$$

Constraint (2.5) is the power demand at any instant t. It is clear that the power demand $P_D(t)$ is supplied by the fuel cell $P_{FC}(t)$ and the battery $P_{BT}(t)$. $P_{BR}(t)$ represents regenerative breaking . Whenever it is positive the battery will be charged as if $P_D(t)$ is decreasing by the amount of regenerative braking. Constraint (2.6) represents the operation limit of a FC. Similarly, constraint (2.7) represents the operational limit of a battery. This is indeed important because charging or discharging some batteries beyond their recommended rating or below their depth of discharging can cause irreversible damage to the health of the battery

14

being used. Constraints (2.8) and (2.9) represent the ramp rate limit of the fuel cell and the battery respectively. Fig. 2.4 shows the different forces acting on the FCHEV.

The power demand $P_D(t)$ is the power needed to push the FCHEV forward. According to [32], $P_D(t)$ can be expressed as:

$$P_D(t) = (F_{ad} + F_r + F_{hc} + F_a)V = F_{te} * V \tag{2.10}$$

Where:

$$F_{ad} = 0.5\rho A_f C_w V^2 \tag{2.11}$$

$$F_r = m_v g(C_{r0} + C_{r1}V)\cos(\delta) \tag{2.12}$$

$$F_{hc} = m_v g \sin(\delta) \tag{2.13}$$

$$F_a = m_v a \tag{2.14}$$

F_{te} is the tractive effort that propels the vehicle forward. F_{te} is equal to the sum of F_{ad} F_r, F_{hc}, and F_a.
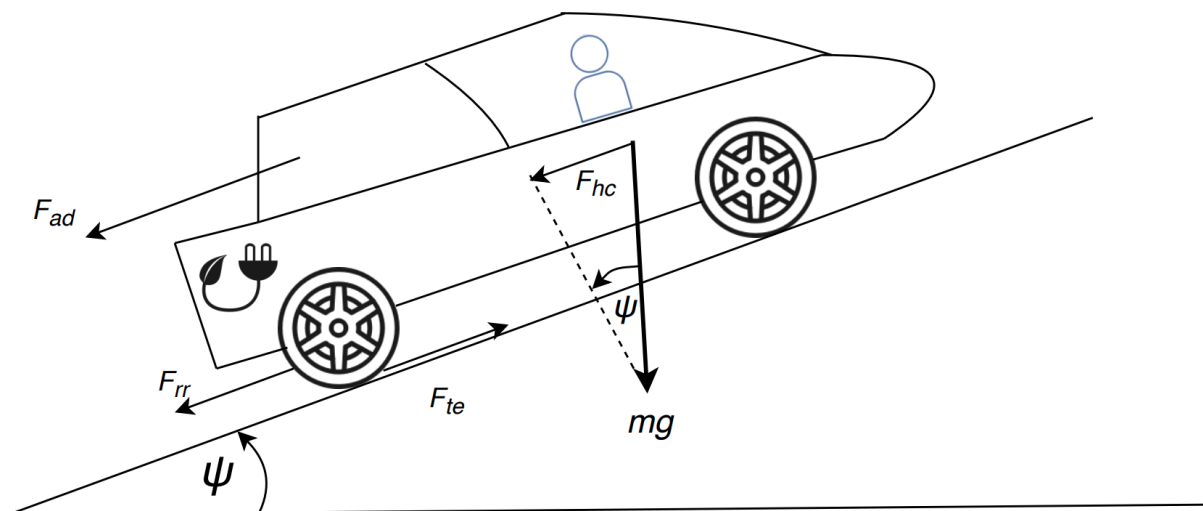
Figure 2.4 Different forces acting on a vehicle

15

CHAPTER III

OPTIMAL OPERATION AND COMPONENT SIZING

A. Optimal Operation

1. Single-Step SSDP Algorithm

The near minimization of ψ is achieved using Single-Stage Dynamic Programming (SSDP), which is inspired from DP and has a similar solution approach. Like DP the power demand is divided into K stages. At each stage k the battery and the fuel cell levels are divided into l states or levels. The limit constraint (2.6) on the FC power is satisfied by setting the maximum and minimum state at any stage equal to F^{max} and F^{min}. The limit constraint on the battery (2.7) , us enforced by introducing a penalty cost on infeasible transitions that violate the SOC or power limits of the battery power. However, unlike DP, SSDP decides on the optimum state at stage k as being the minimum cost transition from the previous stage $k-1$ and, as such, doesn't require a backward trace to select the optimal path that minimizes the cost. It was shown by Karaki et al [29] that this strategy leads to suboptimal solutions. However, the problem is so constrained such that the suboptimal solutions are very close to those obtained using DP. But, the merit of doing so reduces the computation significantly and also allows SSDP to be implemented in real time as an energy management system since it requires only a one stage ahead forecast of the speed.

The SSDP is illustrated in Fig. 3.1 that shows K stages with 4 levels. For example, if we have a FC rated at 100 kW the FC levels could be [0, 33.3, 66.7, 100]. The cost on each arrow is the transition cost and the cost at the top of each state is the cost of the state of the previous stage plus the transition cost, or cost to go. Red circled states represent infeasible transitions due to constraint violation, the transitions to which are penalized. When moving from stage 1 to 2 we have four different transitions: (S_{12}, S_{21}), (S_{12}, S_{22}), (S_{12}, S_{23}), (S_{12}, S_{24});

however, the second transition (S_{12}, S_{22}) has the minimal cost and is thus chosen. This procedure is repeated as we progress forward until stage K, the end of the driving cycle, is reached. The minimum cost at the last stage is the value of ψ sought.
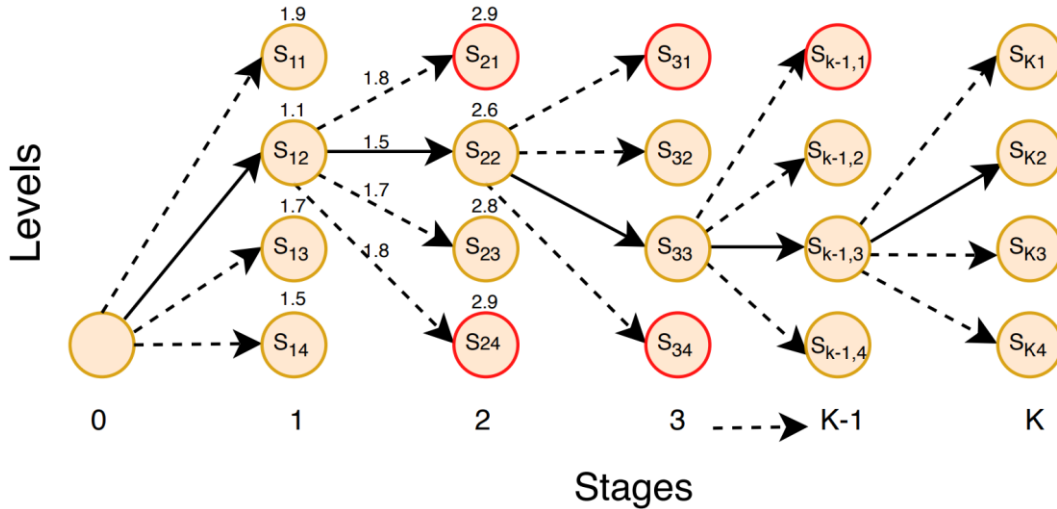
Figure 3.1 Single-Step SSDP Diagram

2. Two-Step SSDP Algorithm

When high accuracy is required, the discretization level has to be smaller, such as a 1 kW in this case, leading to 101 evaluations (for a 100 kW FC) at each stage, as indicated in Fig. 3.2 (a). In the Two-Step SSDP, illustrated in Fig. 3.2 (b), the search space of 101 states is sampled at a courser discretization level, such as 10, leading to 11 states that are evaluated at the first step, i.e. [0 10 20 30 40 50 60 70 80 90 100]. Let the optimal solution at this stage be 63, then in Step 1 the solution that will be found is 60. At the second step another search will be carried out in the neighborhood of 60, i.e. over states [55, 56, 57, 58, 59, 60, 61, 62, 63, 64, 65] to determine the optimal solution of 63. In this manner, the number of evaluations reduces from 101 to 22! This would allow the ability to search much larger spaces in smaller times. This would dramatically reduce the computation time needed to determine the operational cost and thus the optimum design.

17
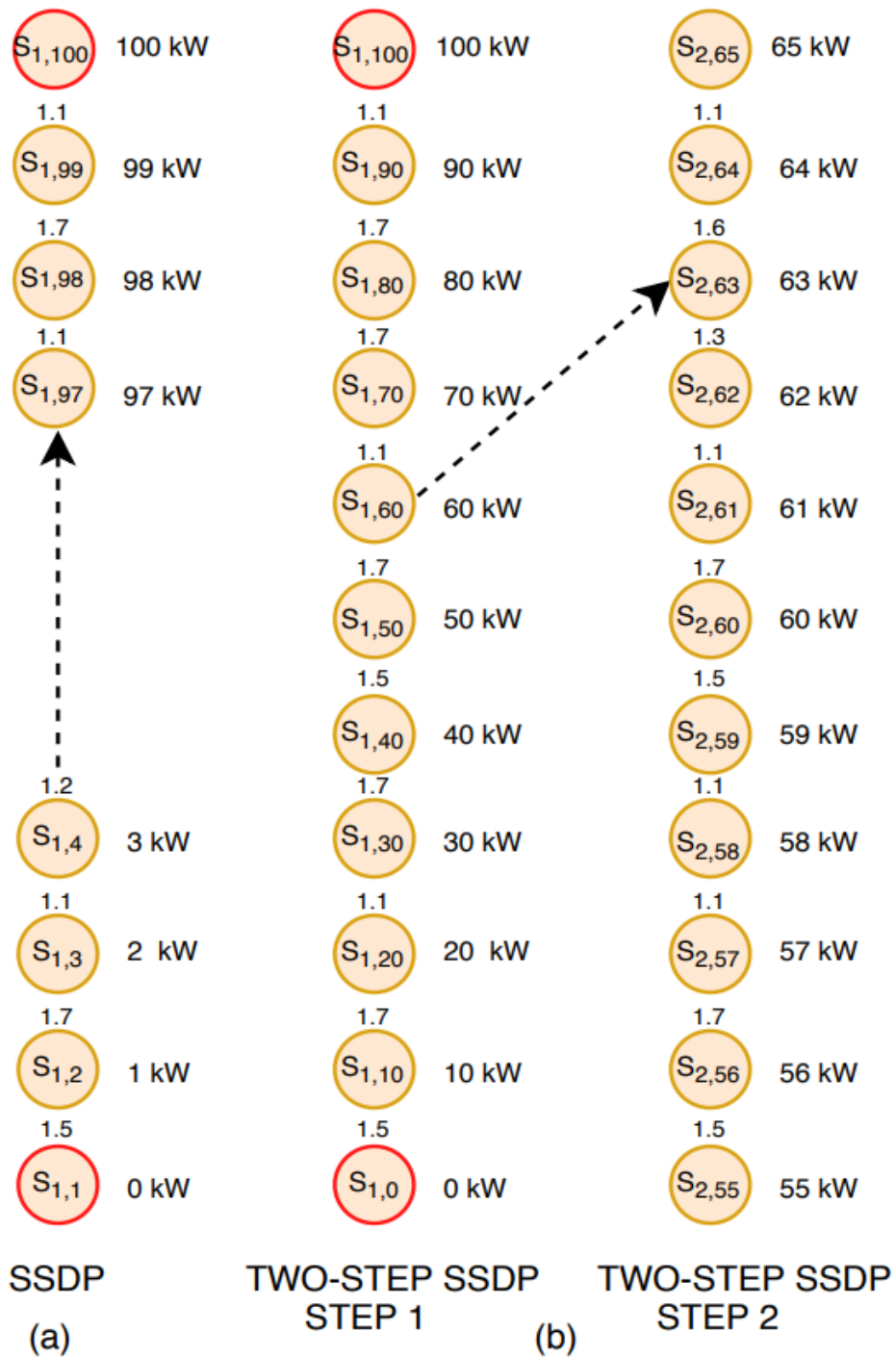
Figure 3.2 Two-Step SSDP Diagram

The pseudo-code of the Two-Step SSDP algorithm is given in List 1.

List 1: Two-Step SSDP Algorithm

---

function $[\widehat{\boldsymbol{S}}, \widehat{\boldsymbol{F}}] = \text{Two\_Step\_SSDP}\,(P_{max}, \Delta P, \Delta t, K, \text{Step\_2} \dots)$

$L = \text{ceiling}(P_{max}/\Delta P) + 1$ "Levels for needed accuracy ΔP

$\Delta P_1 = R_F \Delta t$ "Maximum increment in Step 1

$L_1 = \text{ceiling}(P_{max}/\Delta P_1) + 1$ "Number of levels in Step 1

"Determine fuel cell power levels in Step 1

$\phi_1 = \text{ordered}\,\{j\Delta P_1, j = 0 \dots L_1\}$

$\hat{S}_0 = 0$

"At every stage k

for $k = 1, K$

    "Solve first step

    $[\hat{S}_{k1}, \hat{F}_{k1}] = \text{Solve\_Stage}\,(k, \hat{S}_{k-1}, L_1, \phi_1, \dots)$

    if (Step_2)

        "Determine number of levels in Step 2

        $L_2 = \text{ceiling}(\Delta P_1/\Delta P) + 1$

        "Determine fuel cell power levels in Step 2

        $\phi_2 = \text{ordered}\,\{\hat{F}_k \pm j\Delta P/2, j = 1 \dots L_2\}$

        "Solve second step

        $[\hat{S}_{k2}, \hat{F}_{k2}] = \text{Solve\_Stage}\,(k, \hat{S}_{k-1}, L_2, \phi_2, \dots)$

        "Update set of optimal states up to stage k

        $[\widehat{\boldsymbol{S}}, \widehat{\boldsymbol{F}}]_k = [\widehat{\boldsymbol{S}}, \widehat{\boldsymbol{F}}]_{k-1} + [\hat{S}_{k2}, \hat{F}_{k2}]$

    else

        "Update set of optimal states up to stage k

        $[\widehat{\boldsymbol{S}}, \widehat{\boldsymbol{F}}]_k = [\widehat{\boldsymbol{S}}, \widehat{\boldsymbol{F}}]_{k-1} + [\hat{S}_{k1}, \hat{F}_{k1}]$

    end

end

At every stage, a one-step solution is solved twice. The first step (Step 1) has a reduced number of states L_1 determined by an increment ΔP_1 deduced from the fuel cell ramp rate R_F to preserve the feasibility of transition from one state to the next; let $\Delta P_1 = 10$. With reference to the example shown in Fig. 3.2, the Step-1 solution returns a value of $\hat{S}_{k1} = 7$, corresponding to a fuel power level of $\hat{F}_{k1} = 60$ kW. In Step-2, the number levels is calculated as $L_2 = \text{ceiling}(\Delta P_1/\Delta P) + 1 = 10 + 1 = 11$. The levels are determined in the neighborhood of $\hat{F}_k$ by $\phi_2 = \{55, 56 \dots 64, 65\}$. At Step-2 the solution obtained is $\hat{S}_{k2} = 9$ and $\hat{F}_{k2} = 63$ kW. The function shown in List 1 returns the set of optimal states $[\widehat{\boldsymbol{S}}, \widehat{\boldsymbol{F}}]$ over the given drive cycle.

The algorithm shown in List 2 is used to calculate fuel cell and battery degradation costs for each state l of stage k and whenever the operation, i.e. the transition from state $\hat{S}_{k-1}$ to $S_{k,l}$, is not feasible, then a penalty cost $\mathcal{M}$ is added. Note that $\mathbf{S}$ is the set of feasible transitions. Thus at each stage k, let the minimum cost of stage $k - 1$ be given by $\psi(\hat{S}_{k-1})$. Then the minimum cost of reaching stage k being $\psi(\hat{S}_k)$ is determined recursively by the last "if statement".

List 2: Solve One Stage and Determine Optimum Cost

---

function $[\hat{S}_k, \hat{F}_k] =$ Solve_Stage $(k, \hat{S}_{k-1}, L, \phi \dots)$
    $\hat{S}_k = 1$ and $\psi(\hat{S}_k) = \mathcal{M}$
    for $l= 1, L$
        $F_{k,l} = \phi(l)$ "Fuel cell power"
        $B_{k,l} = \max(D_k - F_{k,l}, B_{min})$ "Battery power
        $C_F = \varphi_F(F_{k,l})$ "Fuel cell cost
        $C_B = \lambda_B \gamma_{avg} \operatorname{sign}(B_{k,l} + 1)/2$ "Battery cost
        $C(\hat{S}_{k-1}, S_{k,l}) = C_F + C_B$ "Transition cost
        "Set large penalty cost $\mathcal{M}$ for infeasible transitions"
        $P_l = 0$
        if $\left((\hat{S}_{k-1}, S_{k,l}) \notin \mathbf{S} \right) \Rightarrow P_l = \mathcal{M}$
        "Minimum cost node in stage k
        if $\left(\psi(\hat{S}_{k-1}) + C(\hat{S}_{k-1}, S_{k,l}) + P_l \right) \leq \psi(\hat{S}_k)$
           $\hat{S}_k = l; \ \hat{F}_k = F_{k,l}$
        end
    end
end

B. Optimal Sizing using Ordinal Optimization

Optimal sizing is based on Ordinal Optimization (OO), which is a structured search procedure to determine the best of N designs with cost $\hat{J}$ as defined by (1). OO is built on two tenets. Firstly, the ordering of different alternatives is more robust against noise than value. In simpler words, consider two designs x and y, where x is better than y. Then if the two designs are evaluated using either a simple model or an accurate model, it is very likely to find out in both cases that x is better than y. The second tenet of OO is that the optimal solution may be very costly to determine in terms of computations and might not be attainable. So in OO a set

of "good enough" solutions is sought, which has a high probability of including the optimum

solution and the best solution in the good enough set is selected [33].

For the design problem being considered in this paper, let the search space of the

optimization variables be Θ that contains all the sizes of the hydrogen tank, fuel cell, battery,

and motor power; and let Θ_N be the set of selected N designs uniformly sampled from the

search space, as illustrated in Fig. 3.3. Note that the green circle represents the real optimum

and the red one represents the estimated optimum i.e. the solution that is good enough and not

costly to achieve.
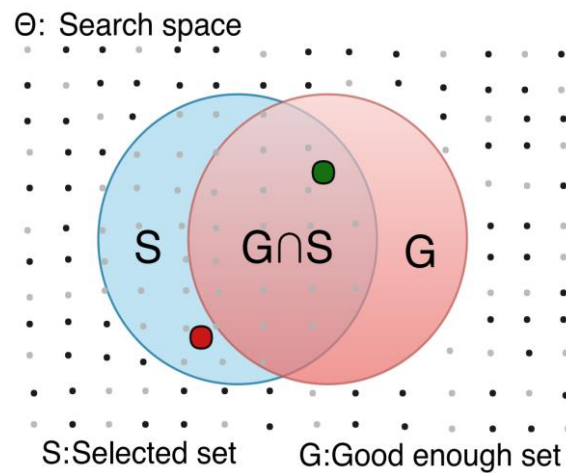
Figure 3.3 Ordinal Optimization Chart

Let G be the "good enough" subset of Θ_N, referred to as the true top-g designs that are

usually unknown. The objective is to select a subset S made of top-s designs in Θ_N, such that

the set of truly good enough designs $(G \cap S)$ has a high alignment probability $AP = P[|G \cap$

$S| \geq k]$ that there are actually k truly good enough designs in S, and k is the alignment level.

The procedure to apply OO for a practical design search problem is as follows:

i)   Sample N designs uniformly from Θ to form Θ_N.
ii) Estimate the performance of the N designs of Θ_N using a simple but computationally
     efficient model and sort them in ascending order.
iii) Plot the Ordered Performance Curve (OPC), which is a bell curve for our car design
     problem.
iv) Specify the size $g= 30$ of the good enough subset (G), the required alignment level ($k=1$),
     and estimate the expected error bound (W).

21

v) Use $Z(k, g) = e^{Z_1} k^{Z_2} g^{Z_3} + Z_4$ with Z_1= 8.1998, Z_2= 1.9164, Z_3= -2.0250 and Z_4= 10 obtained from a table of regression coefficients for AP= 0.95, which correspond to a low error bound of W= 0.5 per unit [10]. The value of Z obtained is 13.7 and thus the size of the selected subset S is 14.

vi) Select the estimated top-s (top-14) designs of Θ_N to form subset (S) and evaluate them using the accurate model.

vii) As per OO theory S contains at least k=1 truly good enough design with a probability level AP $\geq$ 0.95.

The simple model used in step ii) is based on a representative part of the driving cycle and a large discretization step in the SSDP. The different alternatives obtained are then sorted in increasing cost and the "top-s" designs are then selected. In the last step these "top-s" designs are then evaluated using an accurate model that is based on the whole driving cycle and a small discretization step in the Two-Step SSDP. The steps of OO were applied to the design problem being considered with the possible sizes of the hydrogen tank, the fuel cell, the battery and the motor given by the following vectors:

Hydrogen tank (kg) = [1, 2, 3, 4, 5, 6, 7, 8, 9, 10]
Fuel cell (kW) = [10, 20, 30, 40, 50, 60, 70, 80, 90, 100]
Battery (kWh) = [1, 2, 3, 4, 5, 6, 7, 8, 9, 10]
 Motor (kW) = [60, 70, 80, 90, 100, 110, 120, 130, 140, 150]

Based on the different possible sizes, the search space Θ_N then consists of 10,000 different designs. Obviously, the total search space is much larger but it has been trimmed since the best solutions observed in trial run were well within the bounds of the sizes presented above. The simple model was used to evaluate the reduced search space Θ_N then the best among these designs are sorted and the top-s designs are identified. The top-14 good designs selected out of the top-s designs were subsequently evaluated using the accurate model. As a summary of OO operation: first, the search space Θ containing all different component sizes is reduced by sampling to Θ_N containing N designs that are evaluated using a simple model. These designs are then sorted in increasing order of cost. The top-14 designs of Θ_N are then selected and evaluated using an accurate model to yield the best of the good

enough solutions with cost $\hat{J}$ defined by (1). A flow diagram that summarizes the OO

operation is shown below in Fig. 3.4.
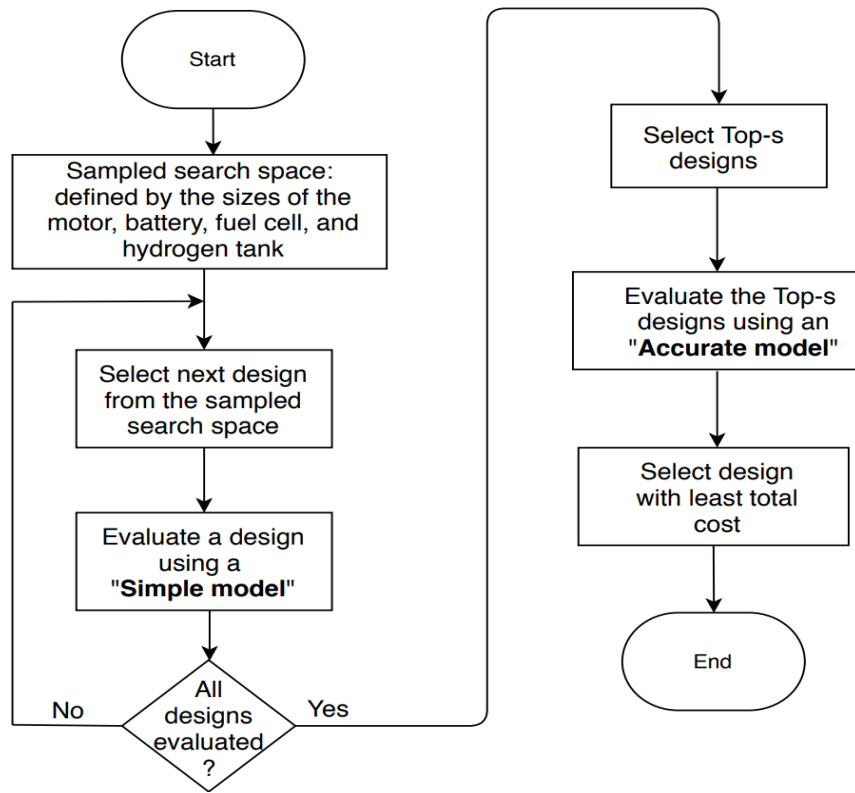
Figure 3.4 Ordinal Optimization Flow Chart

CHAPTER IV

SYSTEM LOSSES AND EFFICIENCY

The electric power train efficiency plays an essential role in the success of an FCHEV design. To further refine our model accuracy, the effect of losses resulting from IM and its drive are modelled and studied in this section.

A. Induction Machine Losses

The three phase induction motor has a big impact on the overall efficiency of the FCHEV. The losses of the IM motor are attributed to core losses, stator and rotor copper losses as well as strass losses. From Fig. 4.1 we can see that the total output power $Pout$ is:

$$P_{out} = P_{in} - (P_{SCL} + P_{Core} + P_{RCL} + P_{Stray} + P_{Friciton}) \tag{4.1}$$

Where P_{in} is the input power, P_{SCL} and P_{RCL} are the stator and rotor copper losses, P_{Core} is the core losses (hysteresis and eddy currents), P_{Stray} is Stray losses (miscellaneous losses), and finally the friction losses are denoted by $P_{Friciton}$.
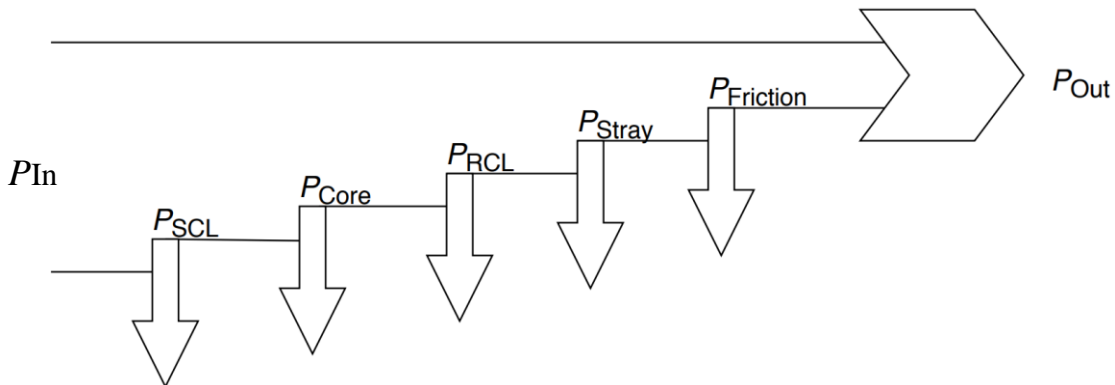
Figure 4.1 Power flow in an Induction Motor

The most significant power losses in the IM are the P_{SCL} and P_{RCL}.

$$P_{SCL} = 3 * I_s * R_s^2 \tag{4.2}$$
$$P_{RCL} = 3 * I_r * R_r^2 \tag{4.3}$$

The stator and rotor copper losses account for more than 50 percent of the IM losses and are

directly related to the current over a given drive cycle. Since current in an FCHEV varies as a function of the drive cycle and the driver's behavior, the P_{SCL} and P_{RCL} will be modelled in a dynamic manner.

The circuit shown in Fig. 4.2 is used to calculate the rotor and stator currents.
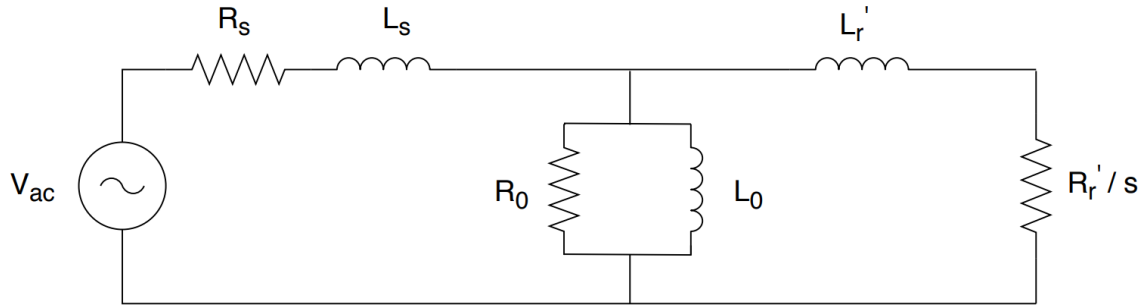
Figure 4.2 Induction motor equivalent circuit

The stator and the rotor current are calculated using the following relations [34]:

$$I_r = \sqrt{\frac{2}{3} \frac{T_e \omega_e}{p} \frac{s}{R'_r}} \tag{4.4}$$

$$I_s = \frac{I_r \sqrt{\left(\frac{R_0 R'_r}{s} - \omega_e^2 L'_r L_0\right)^2 + \left[\omega_e \left(R_0 L_0 + \frac{R'_r}{s} L_0 + R_0 L'_r\right)\right]^2}}{R_0 \omega_e L_0} \tag{4.5}$$

Where p is the number of poles, ω_e is the electrical frequency given rad/sec, s is the slip R'_r and R_s are the rotor and stator resistances respectively. The total current drawn would be equal to the electrical power demand divided by 380 volts. The stator frequency is caluclated from:

$$\omega_e = \frac{\omega_m}{1-s} \tag{4.6}$$

Where ω_m is the mechanical angular frequency of the motor shaft and it is calculated from the speed of the FCHEV. Finally, the electrical torque T_e is calculated dividing the electrical power demand by ω_e.

Table 4.1 shows typical parameters for a 45 kW induction motor. Those paramters are used to calcualte the stator and rotor current, as well as the corresponding stator and rotor copper losses.

Table 4.1 Typical parameters for a 45 kW electric motor [34]

Poles (p)	4
Stator Resistance (R_s)	12 mΩ
Rotor Resistance (R'_r)	12.5 mΩ
Core Resistance (R_0)	14.4 Ω
Stator Leakage Inductance (L_0)	39.5 µH
Rotor Leakage Inductance (L'_r)	41 µH
Magnetizing Inductance (L_0)	2.7 mH

When a motor of differnet size is selected the losses have to be scaled. For example, if in our design a 100 kW motor size is used, the losses would be calculated for the 45 kW motor and then scaled to the acutal motor size (1oo kW in this example). The scaling is done based on the efficiency Table 4.2 which is used for detemrning motors efficiency, and it is provided by the department of energy in the US [35] .

Table 4.2 Motor Size and Efficiency [35]

Motor Size (hP)	Motor Size (kW)	Efficiency
25	19	89.9
30	22	89.3
40	30	90.4
50	37	90.3
75	56	91
100	75	92.1
125	93	91.8
150	112	92.3
200	149	93
250	186	93.1
300	224	93.9

The values in Table 4.2 are converted into watts and are scaled to 45 kW in order to obtain the scaling factor shown in figure 4.3. Fig. 4.3 shows the scaling factor as a function of the motor size. For example if a 45 kW motor is used, the scaling factor would be unity, because the 45 kW motor is our reference valuee. Now if a 100 kW motor is used the losses would be

calculated for the 45 kW and then multiplied by a scaling factor of 0.985. Using Fig. 4.3 a

scaling factor can be interpolated for different motor sizes.
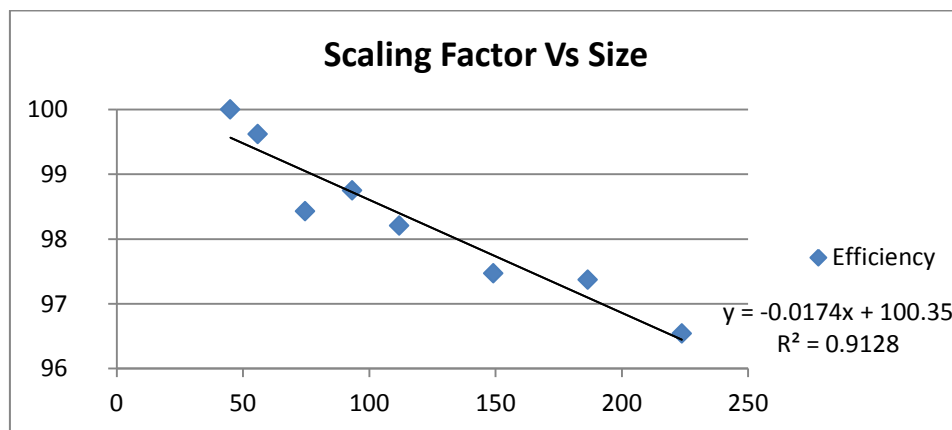
Figure 4.3 Scaling factor vs motor

B. Inverter Losses

Inerter losses can be grouped into two main categories: The active losses and the

passive losses. Active losses are attributed to the semi-conductor devices such as diodes,

IGBTs and MOSFETs. Active losses include conduction losses, switching losses as well

reverse recovery losses. The equivalent circuit for a 6 step inverter is shown in Fig. 4.4.
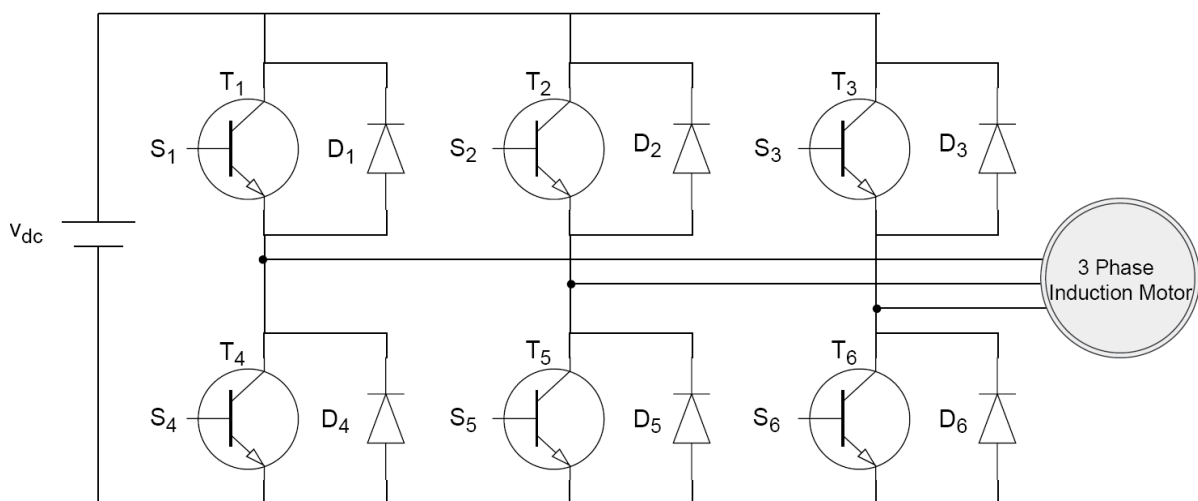
Figure 4.4 Six step inverter

1. Conduction Losses

Conduction losses occur whenever a diode or an IGBT is conducting current. The

power conduction losses in a diode can be accurately calculated using [36]:

$$P_{Diode\_Cl} = 0.026 \frac{T_j+273}{300} (\ln|i| + k_1 i) + k_2 i^2 \qquad (4.7)$$

27

Where k_1= 36.84 and k_2=0.003 and T is the junction temperature given in degrees Celsius.

$$T_j = \Delta T_j + T_a$$

Where T_a is the ambient temperature and ΔT_j is the change in the junction temperature.

$$\Delta T_j = R_{th(j-a)} Pd$$

$R_{th(j-a)}$ is the thermal resistance(junction to ambient) and Pd is the power dissipated in the semi-conductor. The value of Pd can obtained from the diode datasheet (QUIETIR Series 10ETF).

For an IGBT the conduction losses (Watts) will be modelled using [37]:

$$P_{IGBT\_Cl} = U_{ce(SAT)} \, i + R_d \, i^\eta \qquad\qquad (4.8)$$

Where:
$U_{ce(SAT)}$= 1.45 V
R_d = 0.135 Ω
η =1.645

In (4.8) the first term represents the collector emitter saturation voltage, and the second term is for the dynamic resistance. Note that those parameters given are for a 130 A BJT. The size of this power BJT is selected based on the motor current of the FCHEV on the drive cycles. This BJT will be used for different FCHEV designs.

2. Switching Losses

Switching losses account for a remarkable portion of the inverter power losses. For IGBTs we will use the equations below given by [37] at a switching frequency f_s to calculate the switching losses.

$$P_{sw} = f_s * (E_{On} + E_{off}) \qquad\qquad (4.9)$$

$$E_{on} = \frac{1}{6} * V_{dc} * t_r * i \qquad\qquad (4.10)$$

$$E_{off} = \frac{1}{6} * V_{dc} * t_f * i \qquad\qquad (4.11)$$

Where t_r and t_f are the rise and fall time respectively, V_{dc} is the DC link potential. E_{on} and E_{off} are defined as the turn on and turn off energy.

The values of t_r and t_f are obtained from the manufacturers datasheet. In this work Semikron SKM 145GB066D are used for the power IGBTs and the 20 ETF Quiet IR series are used for Diodes.

3. Reverse Recovery Losses

In diodes, power recovery losses appear when a diode switches from its forward conducting state to its reverse conducting one. This can be modelled by [37]:

$$P_{Rr} = \frac{1}{6} * \frac{3}{2} * \frac{Vdc}{2} * t_{rr} * i \tag{4.12}$$

Where t_{rr} is the reverse recovery time.

C. Adding the Losses

Now that we have accounted for the motor and inverter losses we have to make the necessary changes to our power demand constraint. Recall that constraint (2.5) was given by:

$$P_{FC}(t) + P_{BT}(t) - P_{BR}(t) = P_D(t)$$

Where the power demand $P_D(t)$ by the FCHEV was given by

$$P_D(t) = F_{rr} + F_{ad} + F_{hc} + F_{wa} + F_{la} \tag{4.13}$$

Adding the losses that we just modelled to $P_D(t)$ will give us $P_D'(t)$ which can be written as:

$$P_D'(t) = P_D(t) + P_{loss}(t) \tag{4.14}$$

$P_{loss}(t)$ is the sum of all the losses calculated previously. This includes all conduction losses, switching losses and reverse recovery losses.

$$P_{loss}(t) = P_{Cl} + P_{Sw} + P_{Rr} \tag{4.15}$$

Where P_{Cl} is the sum of conduction losses defined earlier.

CHAPTER V

SIMULATION OF AN FUEL CELL HYBRID ELECTRIC VEHICLE

So far we have modelled the FHCEV by the equations that govern its power demand and its dynamics. We have also set the necessary constraints on the different design variables. Consequently, an optimal sizing and optimal operation methodology have been set. In this chapter we are going to simulate the performance of the FCHEV and test the effect of losses on the power demand, on the sizing of components and other variables of interest. The UDDS and the HWFET drive cycles were used in weighted mix to determine the operating costs of the vehicle design. These drive cycles are shown in figures 5.1 and 5.2 respectively.
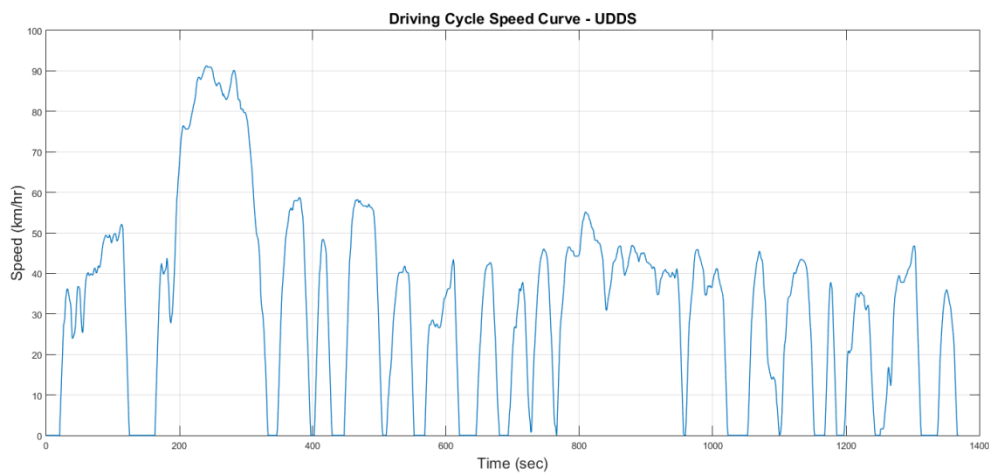
Figure 5.1 UDDS drive cycle
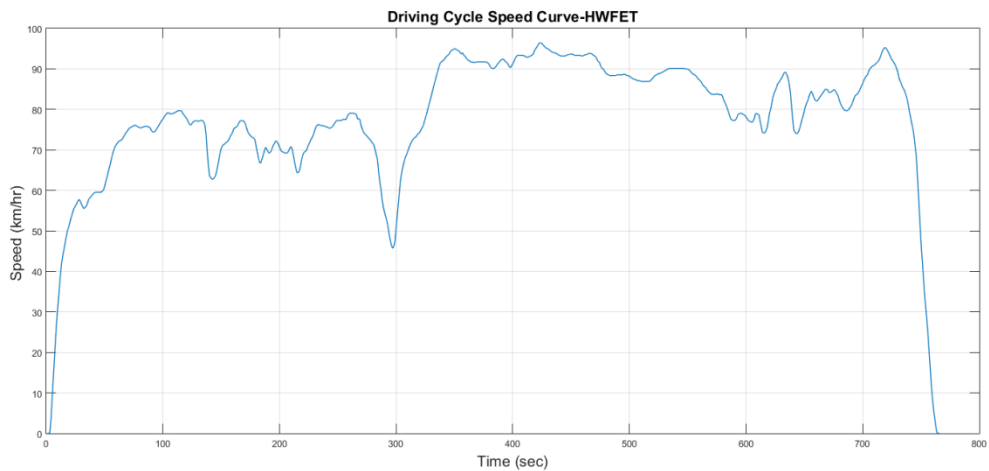
Figure 5.2 HWFET drive cycle

The costs of the design components associated with the glider, motor as well as others are summarized in Table 5.1. These costs will be used in the operational and investment cost calculations. Similarly, Table 5.2 shows the technical specifications and design parameters of the advanced FCHEV to be simulated. The possible set of components sizes for this FCHEV are shown in the sampled search space below.

Table 5.1 Vehicle Design Cost Data

Glider Cost	C_G	23250
Motor Cost	C_M	$52/kW
Fuel Cell Cost	C_{FC}	$40/kW
Hydrogen Cost	C_{H2}	$14/kg
Hydrogen Tank Cost	C_T	$1700/kg
Battery Cost	C_{BT}	180/ kWh

Table 5.2 Technical Specification and Design Parameters for the Advanced FCHEV

Length	L	4.8 m
Height	H	1.610 m
Frontal area	A_f	2.18 m^2
Air drag coefficient	C_d	0.28
Coefficient of rolling resistance	C_{r0}	0.0055
Coefficient of rolling resistance	C_{r1}	0.00023
Wheel radius	W_r	0.317 m
voltages at high bus	V	380 V
Efficiency of electric motor	η_m	0.9025
Efficiency of electric motor (braking)	η_b	0.85

Sampled search space for the fuel cell hybrid electric car:

 Hydrogen tank sizes= [1, 2, 3, 4, 5, 6, 7, 8, 9, 10]* 1000 (kg)

 Fuel cell sizes = [10, 20, 30, 30, 40, 50, 60, 70, 80, 90, 100] (kW)

 Battery sizes= [1, 2, 3, 4, 5, 6, 7, 8, 9, 10] (kWh)

 Motor sizes= [90, 95, 100, 105, 110, 115, 120, 125, 130] (kW)

As described earlier the sampled search is a subset of the global search space. This sampled search space has 10,000 designs (using the multiplicative rule). Each design will be evaluated using a simple model. The evaluated designs will then be sorted in decreasing order based on the objective cost function. Finally, the top wining designs obtained using the simple model will be evaluated using an accurate one. In the first simulations the charge sustaining mode is

used. The fuel cell energy and the battery remaining energy are shown in Fig 5.3 (a). The

battery on both cycles is acting as a buffer and has almost a constant SOC at 0.82 (b). Thus

the energy is being supplied from the fuel cell throughout both cycles, which is shown by the

decreasing curve on both cycles in Fig. 5.3 (a).
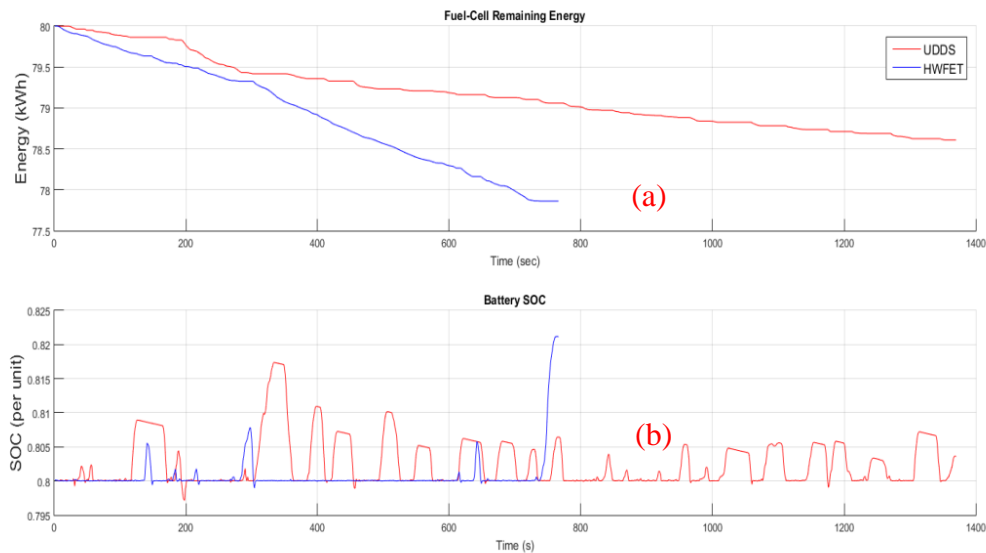
Figure 5.3 Fuel cell and battery level on the UDDS and HWFET cycles

The results for the advanced design exercise using the simple model are summarized in Table

5.3. Note that losses here are included, but as a fixed quantity, the FCHEV has an 85 percent

efficiency.

Table 5.3 Design Results for Normal Advanced FCHEV Using Simple Model

Run Number	H2 Tank Size (g)	Fuel-Cell Size (kW)	Battery Size (kWh)	Motor Size (kW)	Total Car Mass (kg)	Investment Cost ($/year)	Operation Cost ($/year)	Objective Cost ($/year)	Infeasibility Level
1	5000	40	3	110	1499	3094	3207	6784	0
2	5000	40	4	110	1511	3111	3220	6818	0
3	5000	50	3	110	1521	3132	3198	6820	0
4	6000	40	3	110	1508	3115	3223	6825	0
5	5000	40	3	115	1504	3119	3222	6828	0
6	5000	40	4	115	1516	3136	3226	6852	0
7	6000	40	3	115	1513	3140	3222	6853	0
8	5000	40	5	110	1523	3128	3237	6855	0
9	5000	50	4	110	1533	3149	3215	6857	0
10	5000	40	3	120	1508	3144	3223	6858	0
11	6000	40	4	110	1520	3132	3236	6859	0
12	5000	50	3	115	1526	3157	3211	6861	0

According to the simple model the winning design has the following set of components:
A 5 kg hydrogen tank, a 40 kW fuel cell, a 3 kWh battery, and a 110 kW motor. Now the top
25 designs in the simple model are evaluated again but using the accurate model. Only the
first 20 designs are summarized in Table 5.4. The optimal design obtained using the accurate
model is the same as the one obtained using the simple model. The second best design is also
the same.

Table 5.4 Design Results for advanced FCHEV Using Accurate Model (Losses Included as a Fixed Number)

Run Number	H2 Tank Size (g)	Fuel-Cell Size (kW)	Battery Size (kWh)	Motor Size (kW)	Total Car Mass (kg)	Investment Cost ($/year)	Operation Cost ($/year)	Objective Cost ($/year)	Infeasibility Level
1	5000	40	3	110	1500	3094	2956	6533	0
2	5000	40	4	110	1512	3111	2969	6567	0
5	5000	40	3	115	1504	3119	2961	6568	0
4	6000	40	3	110	1509	3116	2967	6569	0
3	5000	50	3	110	1522	3132	2959	6581	0
8	5000	40	5	110	1523	3129	2983	6601	0
6	5000	40	4	115	1516	3136	2975	6601	0
10	5000	40	3	120	1509	3144	2967	6602	0
11	6000	40	4	110	1521	3133	2981	6604	0
7	6000	40	3	115	1513	3141	2972	6604	0
15	7000	40	3	110	1518	3137	2978	6605	0
9	5000	50	4	110	1533	3150	2971	6613	0

This in fact reflects how accurate the simple model is and opens the door for further
investigation on how much further the simple model can be "enhanced". In other words, it
looks like the already simple model can be further simplified by using even a smaller portion
of the driving cycles or a lesser number of levels.

Now that the best design is obtained and verified using the accurate model, we are going to
include the losses on the accurate model and identify their effect on the design obtained. The
simulation runs performed above will now be repeated using the same approach and the same
design and cost parameters; however, the power demand constraint will now include the
different losses in the electric power train as discussed in chapter four .The motor electric
current drawn on the UDDS cycle is shown in Fig. 5.4.
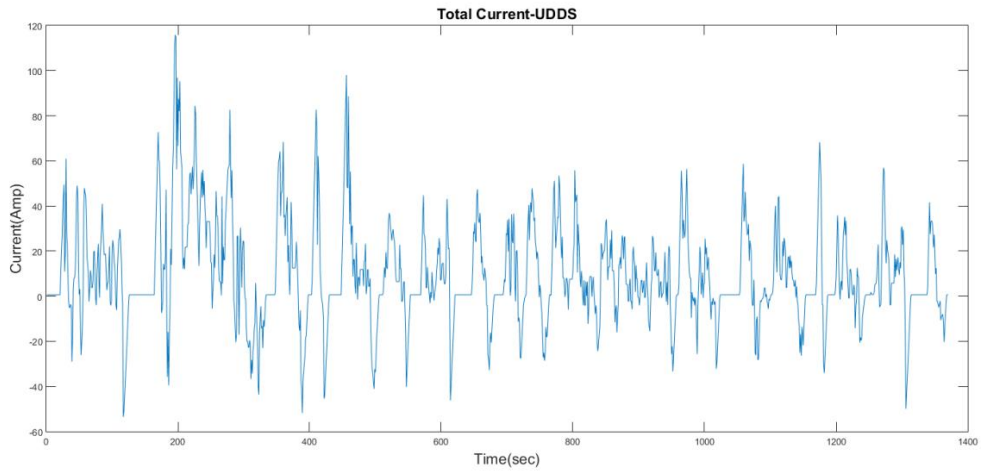
Figure 5.4 Total motor current on the UDDS cycle

From the current waveforms the losses of the electric train are calculated. The total motor

losses for instance are shown in Fig. 5.5.
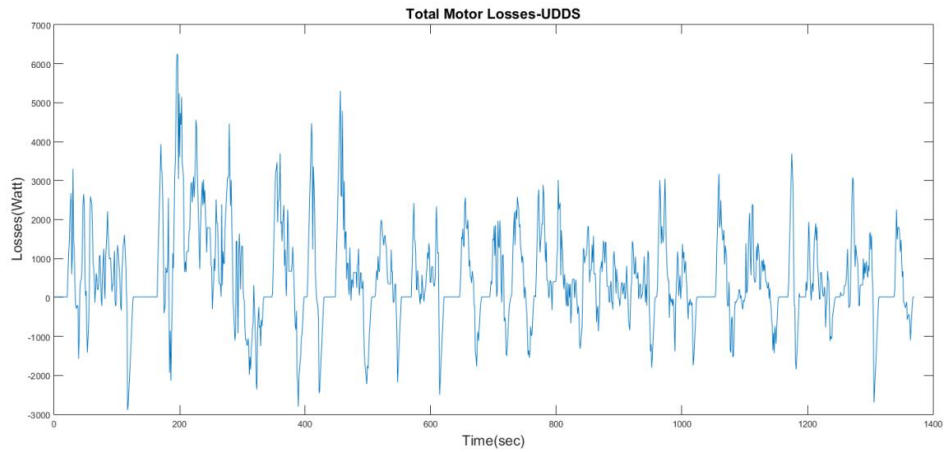
Figure 5.5 Total motor losses on the UDDS cycle

Similarly the total losses in the IGBT and the diode components are shown in Fig. 5.6 and

Fig. 5.7 respectively.
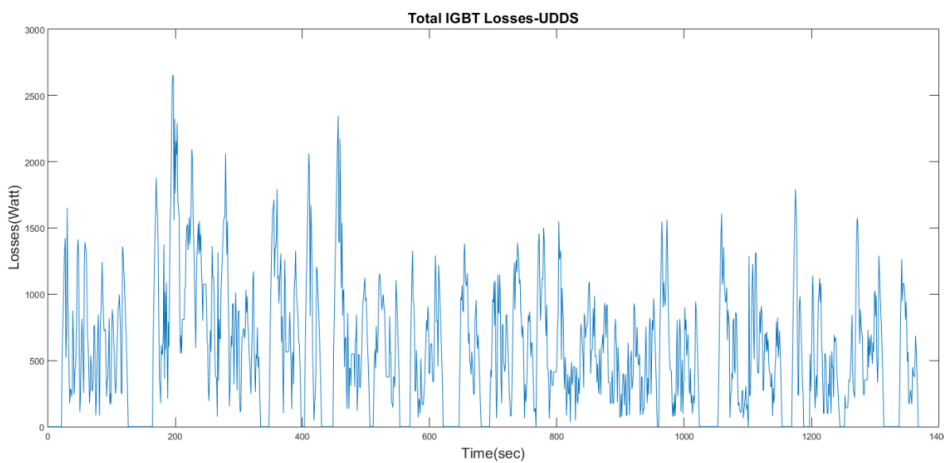
Figure 5.6 Total IGBT losses on the UDDS cycle

34
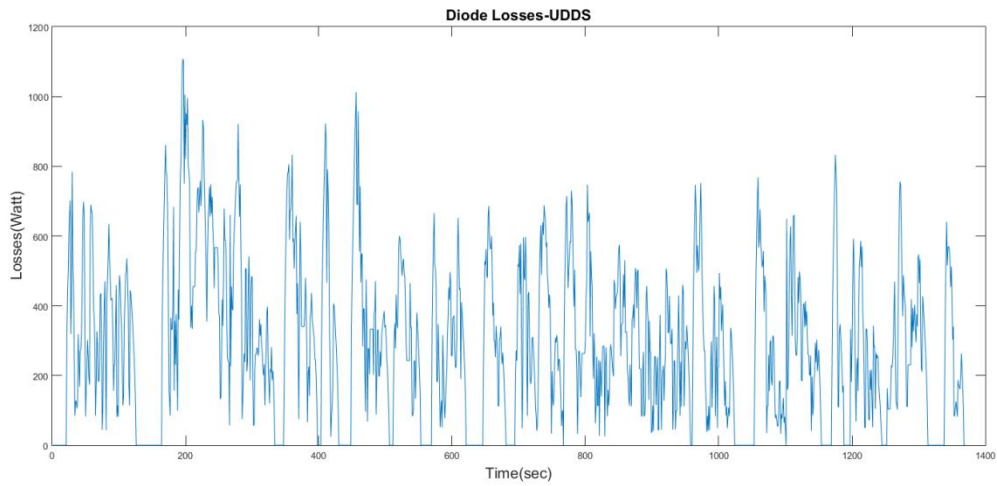
Figure 5.7 Total Diode losses on the UDDS cycle

Now the same losses are calculated for the HWFET cycles. The total motor current drawn on the HWFET cycle is shown in Fig. 5.8. Then the total motor losses, the IGBT, and diode losses are shown in Fig. 5.9, 5.10 and 5.11 respectively.
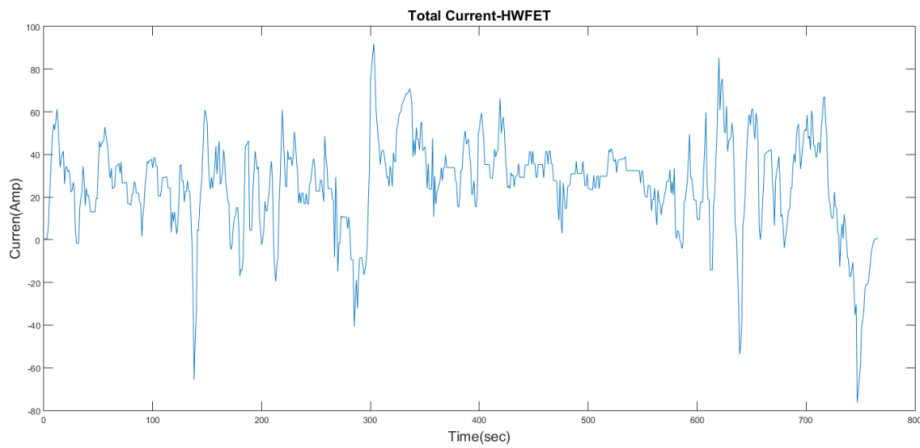
Figure 5.8 Total motor current on the HWFET
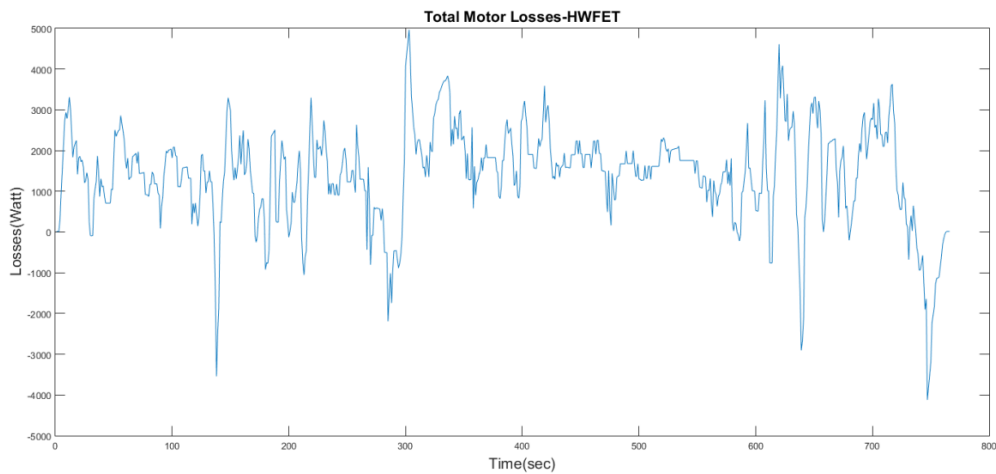
Figure 5.9 Total motor losses on the HWFET

35
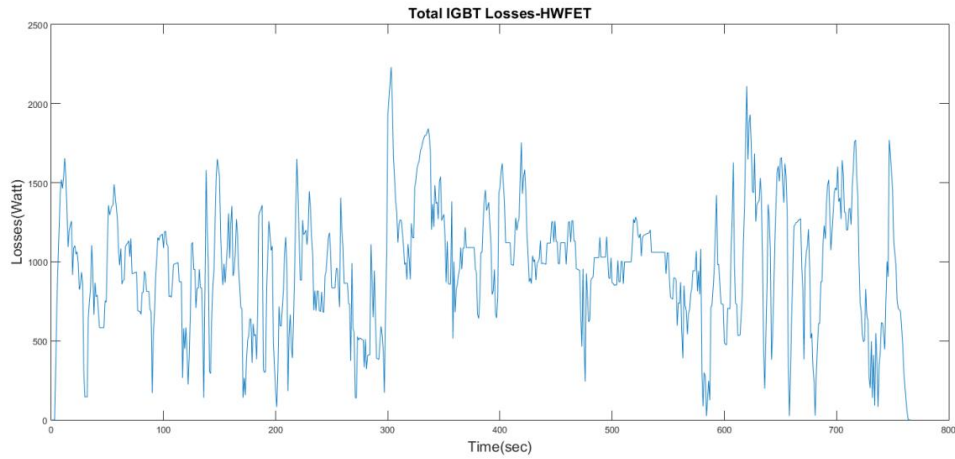
Figure 5.10 Total IGBT losses on the HWFET
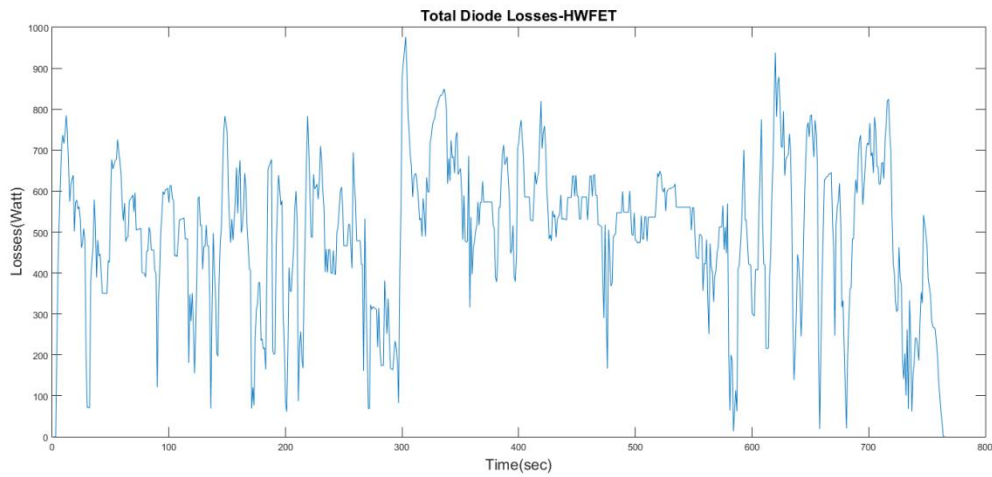
Figure 5.11 Total diode losses on the HWFET

Table 5.5 summarizes the losses on the HWFET and UDDS driving cycles. Note that the losses on the UDDS cycle are higher than that of the HWFET which is totally reasonable. This is because first the HWFET has less regenerative braking that the UDDS and second the speed profile over the HWFET is higher than that on the UDDS. Consequently, the HWFET has higher conduction losses as most of the power demand throughout the whole drive cycle is positive.

Table 5.5 Energy Losses Summary on the HWFET and UDDS

	HWFET	UDDS
Total motor losses	1405	510
Total IGBT losses	962.4	564
Total diode losses	496.5	288.4

Table 5.6 below shows the design for a normal FCHEV using accurate model with losses included. Note that the losses have not been included in the simple model. The top design when the losses are included is still the same as the one obtained without losses in table 5.4.

Table 5.6 Design Results for Advanced FCHEV Using Accurate Model (Dynamic Losses Included)

Run Number	H2 Tank Size (g)	Fuel-Cell Size (kW)	Battery Size (kWh)	Motor Size (kW)	Total Car Mass (kg)	Investment Cost ($/year)	Operation Cost ($/year)	Objective Cost ($/year)	Infeasibility Level
1	5000	40	3	110	1500	3094	3925	7503	1
3	5000	50	3	110	1522	3132	3893	7515	0
13	5000	60	2	110	1532	3154	3884	7531	0
5	5000	40	3	115	1504	3119	3932	7539	1
2	5000	40	4	110	1512	3111	3943	7542	1
4	6000	40	3	110	1509	3116	3940	7543	1
12	5000	50	3	115	1526	3157	3900	7550	0
9	5000	50	4	110	1533	3150	3910	7552	0
14	6000	50	3	110	1531	3154	3907	7554	0
29	5000	60	3	110	1543	3171	3897	7563	0
10	5000	40	3	120	1509	3144	3939	7575	1
6	5000	40	4	115	1516	3136	3950	7577	1

Infeasibility Level: 1 due to Low Ramp Rates or Energy Limits
Infeasibility Level: 2 due to Capacity Shortage
Infeasibility Level: 3 due to fuel Cell Level
Infeasibility Level: 4 due to design range

However, there are two important remarks here. Firstly, the same design now has an infeasibility level 1. An infeasibility level 1 is automatically generated in the program whenever the power demand or ramp rate limit constraints are violated. Since power demand is now bigger recall that from (4.11):

$$P'_D(t) = P_D(t) + P_{loss}$$

Secondly, we notice that the yearly objective function is now $ 7503 per year compared to $ 6533 per year. Going back to the infeasibility level, we can no longer consider the first design in the accurate model to be a feasible design. The power demand constraints are not soft constraints and thus they cannot be violated. In this case, the second best design is to be chosen. From table 5.6 the second best design would have a 5 kg hydrogen tank, a 5- kW FC size, a 3 kWh battery and a 100 kW motor size. Notice that the only difference in best design

with and without losses only differs in the size of the selected fuel cell size. However, since
the losses average value is around 3 kW, it would be interesting to investigate smaller fuel
cell size within the 40 kW range using a step of 1 kW. Therefore we will repeat the above
simulation using the following search space:

Hydrogen tank sizes= [1, 2, 3, 4, 5, 6, 7, 8, 9, 10]* 1000 (kg)
Fuel cell sizes = [40,41,42,43,44,45,46,47,48,49,50] (kW)
Battery sizes= [1, 2, 3, 4, 5, 6, 7, 8, 9, 10] (kWh)
Motor sizes= [90, 95, 100, 105, 110, 115, 120, 125, 130] (kW)

After repeating the simulation under the same conditions described before, we see that the
winning design from table 5.7 will have the same parameters as before except for a the FC
size. The FC size is now 44 kW. This number actually is expected as the average value for
the losses was around 3 kW. Thus, we will need a 4 kW bigger FC size to accommodate for
the losses.

Table 5.7 Design Results for Advanced FCHEV Using Accurate Model (Dynamic Losses Included Small Increments)

Run Number	H2 Tank Size (g)	Fuel-Cell Size (kW)	Battery Size (kWh)	motor Size (kW)	Total Car Mass (kg)	Investment Cost ($/year)	Operation Cost ($/year)	Objective Cost ($/year)	Infeasibility Level
4	5000	44	3	110	1509	3109	3907	7502	0
2	5000	42	3	110	1504	3102	3915	7502	1
3	5000	43	3	110	1506	3106	3911	7503	1
1	5000	40	3	110	1500	3094	3925	7503	1
5	5000	45	3	110	1511	3113	3904	7504	0
6	5000	46	3	110	1513	3117	3901	7505	0
8	5000	47	3	110	1515	3121	3899	7508	0
7	5000	48	3	110	1517	3125	3895	7509	0
18	5000	49	3	110	1519	3129	3894	7511	0
12	5000	50	3	110	1522	3132	3893	7515	0
11	5000	42	3	115	1509	3127	3921	7537	1
24	5000	44	3	115	1513	3134	3914	7538	0

CHAPTER VI

SIMULATION AND DESIGN of an FCHEV USING LIGHT MATERIAL

Designing lighter HEVs results in a remarkable decrease in power demand as well as in fuel consumption. In fact, up to 5 to 8 % fuel reduction can be obtained by reducing the vehicle weight by 10 %. When it comes to air pollution, a 100 kg reduction in a weight will reduce the emitted CO_2 by 12.5 g/km [38]. In order to obtain lighter mass, we will need to incorporate materials having less mass density than steel/iron. In fact, steel still dominates till this day the mass composition of a traditional car. Aluminum, for instance, is a top candidate which is highly being researched as a promising successor to steel and is more likely to occupy a large percentage of a car mass composition especially in HEVs. According to [39], "magnesium, titanium, and glass as well as carbon fiber reinforced plastics" are also potential competitors and are more likely to be incorporated into the composition of new HEVs.

A. Modelling and design

Our first design will serve as a baseline model, in which the body of the FCHEV is based on a Toyota Venza (2009). In the second model which will serve as the advanced model the body of the FCHEV is based on a reduced one proposed by Lotus engineering research group [40]. The body of the baseline FCEHV as seen from the pie chart in Fig. 6.1 is mainly composed of steel/iron 67% while the plastic and aluminum used are only 14%. Similarity Fig. 6.2 shows the mass composition of the advanced design. The mass of each component of both FCHEVs can be seen in Table. 6.1. In Table 6.2 the technical specification and design parameters for both FCHEVs are listed. To study solely the effect of weight reduction both vehicles will have same dimensions and physical parameters and only the mass and the size of components will differ between the baseline and the advanced design.
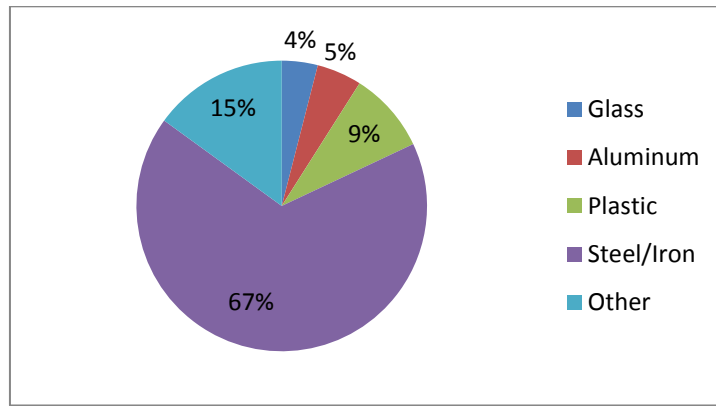
Figure 6.1 Body composition of baseline FCHEV
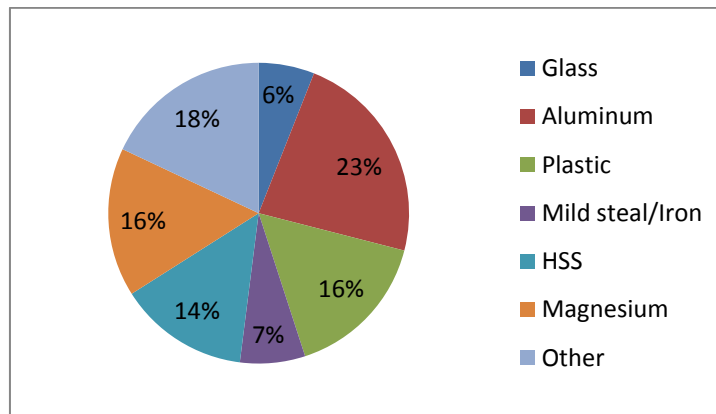
Figure 6.2 Body composition of a light weight FCHEV

In the lighter body, we can see from the pie chart in Fig. 6.2 that plastic and aluminum constitute around 39 % of the total body mass while mild steel and iron are only 7%. The total body mass of the Light FCHEV is 793.8 kg. The use of such light materials allowed lotus engineers to reduce the total body mass by around 38.4 % (495.8 kg) with a projected cost factor increase of 1.03 only. This is due to the fact that although some material used are more expensive than steel/iron, the significant mass reduction offsets the price increase in the advanced body.

Table 6.1 Mass Reduction and Cost Index Comparison

	Baseline	**Light weight body**	**Mass reduction**	**Cost index**
Components	**Mass (kg)**			
Body	382.5	221.1	161.4	1.4
Closures/Fenders	143.2	83.9	59.1	0.7
Bumpers	17.9	17.9	0	1.1
Thermal	9.25	9.25	0	1
Electrical	23.6	15.1	8.6	0.96
Interior	250.6	153	97.6	0.96
Lighting	9.9	9.9	0	1

Suspension/Chassis	378.9	217	161.9	0.95
Glazing	43.71	43.71	0	1
Miscellaneous	30.1	22.9	7.2	0.99
Total (kg)	1289.53	793.76	495.77	1.03

Table 6.2 Technical Specification and Design Parameters for Both FCHEVs

Length	L	4.8 m
Width	W	1.905 m
Height	H	1.610 m
Frontal area	A_f	2.607 m^2
Air drag coefficient	C_d	0.33
Coefficient of rolling resistance	C_{r0}	0.0055
Coefficient of rolling resistance	C_{r1}	0.00023
Wheel radius	W_r	0.2413 m
voltages at high bus	V	650 V
Efficiency of electric motor	η_m	0.9025
Efficiency of electric motor (braking)	η_b	0.85

Fig. 6.3 shows the power demand by the baseline FCHEV as well as the reduced FCHEV over the highway driving cycle. It is obvious that the power demand of the baseline FCHEV shown is higher than that of the reduced FCHEV especially at high peaks.
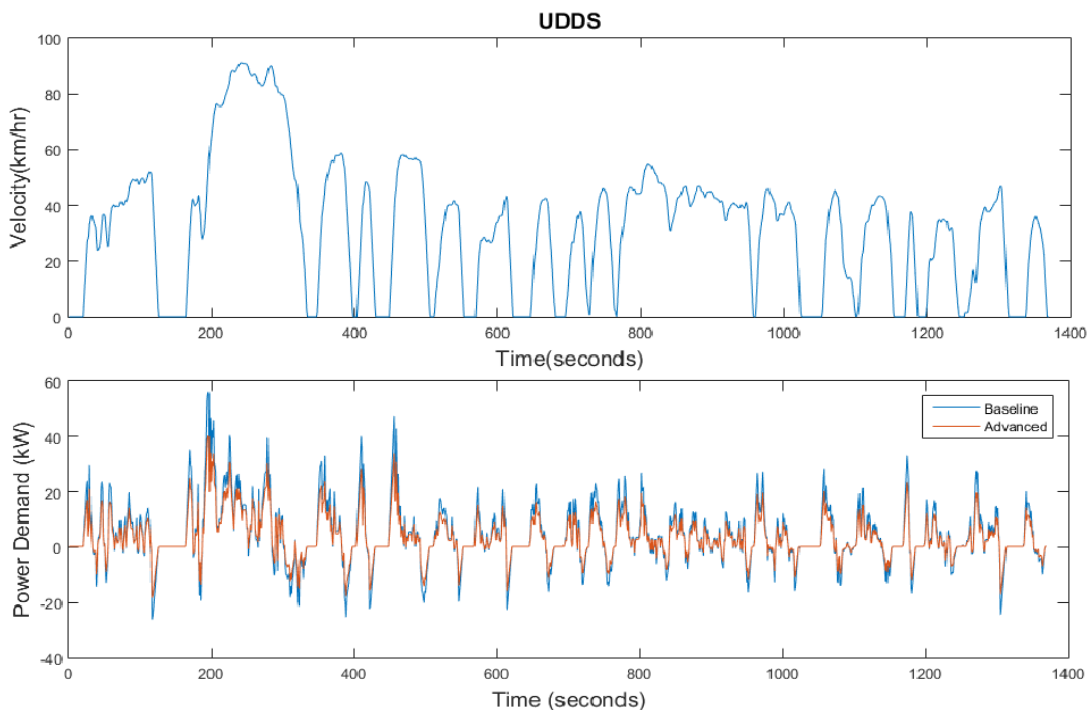
Figure 6.3 Power demand of both FCHEVs on the UDDS driving cycle

Table 6.3 summarizes the results obtained on the UDDS cycle. Remarkable savings are achieved in terms of hydrogen consumption, as well in the operation cost as a whole. Moreover, the light FCHEV has an improved MPGGE.

41

Table 6.3 Simulation Summary on UDDS Cycle

	Baseline	Advanced	Savings (%)
H2 Consumption (g/trip)	104.8	80.7	23
MPGGE	71.0	92.1	29.8
Fuel-Cell Hydrogen Cost ($/ year)	2200	1695	23
Battery Degradation Cost ($/ year)	121	81	32.7
Adjusted Operation Cost ($/ year)	3315	2537	23.5

The simulation of both designs is repeated now over the HWFET cycle. The power demand of both cars is shown in Fig. 6.4 Again the power demand of the light FCHEV is less than that of the baseline FCHEV.
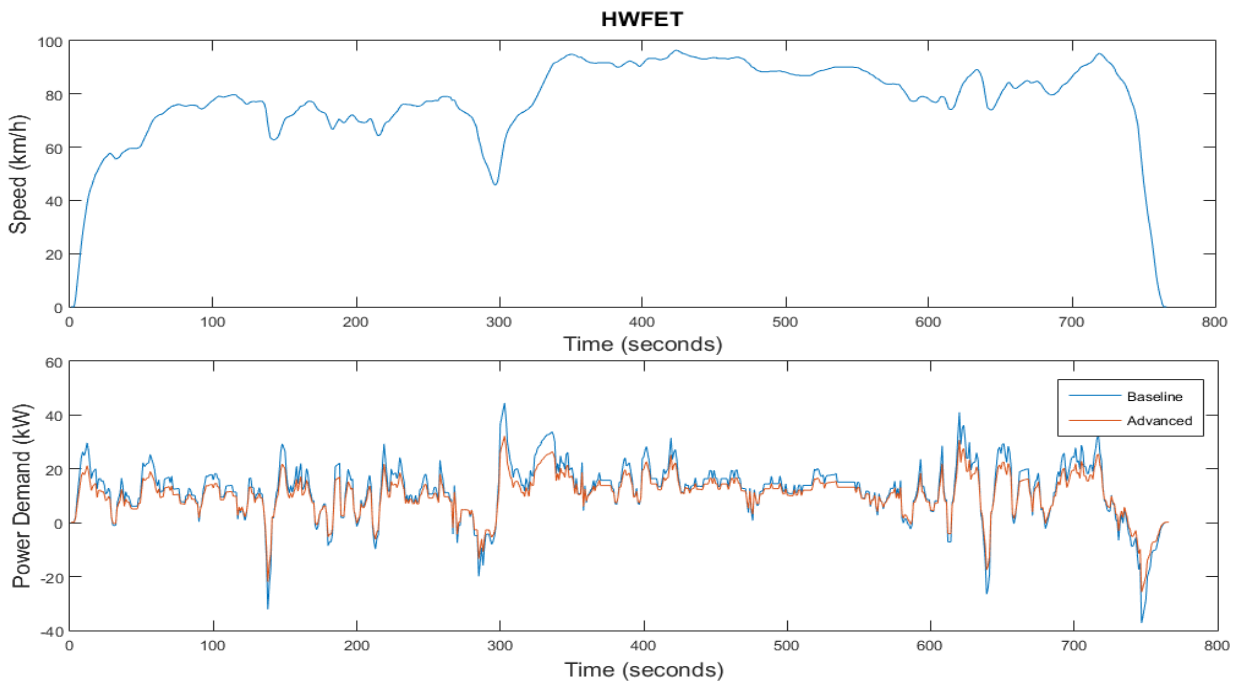
Figure 6.4 Power demand of both FCHEVs on the HWFET driving cycle

Table 6.4 shows a summary of the results obtained on the HWFET cycle. Again remarkable savings are obtained in terms of hydrogen consumption and operation cost.

Table 6.4 Simulation Summary on HWFET Cycle

	Baseline	Advanced	Savings (%)
H2 Consumption (g/trip)	151.3	128.4	15.1
MPGGE	67.6	79.7	17.8
Fuel-Cell Hydrogen Cost ($/ year)	3176	2697	15.1
Battery Degradation Cost ($/ year)	29.9	18.9	36.7
Adjusted Operation Cost ($/ year)	4580	3880	15.3

Two similar FCHEV are simulated also using the Advanced Vehicle Simulator (ADVISOR). The simulation was repeated two times on the HWFET: once to account for the baseline design, and once to account for the advanced design. The same work was repeated on the UDDS cycle. To simulate a design similar to the baseline design or the advanced one, one has to choose a fuel cell car having the same architecture, same mass and other similar properties.

The results from ADVISOR are summarized in table 6.5 The results show a 15.1 percent savings on the HWFET, and 23 percent savings on the UDDS cycle. The MPGGE on the HWFET is for the baseline design is 67.6 using our simulation tool, and 70.1 using ADVISOR. For the advanced design the MPGGE, was 79.7 using our tool and 82.6, using ADVISOR. Values and savings are also verified on the UDDS cycle for both designs.

Table 6.5. Summary of Results Using ADVISOR

	UDDS		HWFET	
Tool	Simulation-tool	ADVISOR	Simulation-tool	ADVISOR
Percentage in savings (%)	15.1	15.1	23	24.6

The results are as expected and the savings are verified and the error in the case of HWFET is 0 % and on the UDDS is 1.6 %. In fact, both our program and ADVISOR show significant savings by more than 10 percent in hydrogen consumption.

Although the results obtained are as expected, the question remains whether the cost of using more expensive light material will be offset by the savings obtained from using these materials. To answer this question we take a look at table 6.6 which summarizes the design results for the advanced FCHEV. The winning advanced design has a 5 kg tank, a 40 kW FC size, a 3 kWh battery and a 100 kW motor size. We then proceed and repeat the same simulation for the baseline design.

Table 6.6 Design Results for Advanced FCHEV Using Accurate Model

Run Number	H2 Tank Size kg	Fuel-Cell Size kW	Battery Size kWh	Motor Size kW	Annual Investment Cost $/ year	Annual Operation Cost $/year	Total annual Cost $/year
1	5	40	3	100	3157	3275	6926
2	6	40	3	100	3184	3287	6968
3	5	40	4	100	3196	3291	6986
4	5	40	3	110	3207	3288	6996
5	7	40	3	100	3210	3299	7010
6	6	40	4	100	3222	3303	7028
7	6	40	3	110	3233	3299	7038
9	5	50	3	110	3252	3291	7051
8	5	40	4	110	3246	3303	7055
10	5	40	3	120	3257	3299	7065

The results of both the light and the advanced design are summarized in table 6.7. From table 14 we notice that the powertrain components of the advanced design are less than those of the baseline. Moreover, we see that operational and investment cost and consequently the total cost of the advanced design are less than those of the baseline design.

Table 6.7 Results Summary of Design Parameters and Cost Elements

	Baseline	Advanced	Savings (%)
H2 Tank Size (kg)	6	5	16.7
Fuel-Cell Size (kW)	60	40	33.3
Battery Size (kWh)	4	3	25
Motor Size (kW)	140	100	28.6
Annualized Investment ($/ year)	3512	3157	10.1
Annual Operation ($/year)	4017	3275	18.5
Total Annual Cost ($/year)	8071	6926	14.2

Despite the fact that the glider cost of the advanced design is higher by 3 % than that of the baseline design, we can conclude that although light materials may seem more expensive than conventional ones. In fact, the savings in components sizes, power demand and the use of less material to occupy the same volume will offset the cost and make the advanced design less expensive.

The design exercise above was performed using three optimal operation strategies. The time recorded to run the simple and accurate model was recorded. The near optimal design obtained using DP, SSDP, and the Two-Step SSDP, were the same; however, the simulation time is significantly reduced when SSDP is used instead of DP for the accurate model. The simulation time for the accurate model is further reduced by using the Two-Step SSDP. The computation time in CPU is summarized in table 6.8. Despite the remarkable savings in computation time, the costs of operation obtained using the three different methods was consistent and almost equal.

Table 6.8 Computation Time in CPU for Different Methods

	DP	SSDP	Two-Step SSDP
Simple Model (10,000 Designs)	394.0	177.4	177.4
Accurate Model (Top-14 Designs)	58.2	28.2	12.2
Total Time (seconds)	452.2	205.6	189.6

CHAPTER VII

FCHEV DESIGN AND THE ENVIROMENTAL ASPECT

The emergence of Hybrid Electric Vehicles is mainly motivated by the environmental benefits that they claim to offer. This chapter aims to investigate the carbon foot print of FCHEV when being operated in a charge sustaining, and in a charge depletion mode. In the latter case, the FCHEV will act as an electric vehicle. Moreover, the carbon foot print of the FCHEV will be compared to internal combustion engine vehicles (ICEV) of the same class. The well to wheel (WTW) analysis aims to calculate the greenhouse gas emissions that are usually associated with the transportation sector.

A.WTW for an ICEV

For an internal combustion engine, the WTW is divided into two major parts: extracting the oil, refining it, transporting it and delivering it to fuel station and thus to the car tank (well to tank). The second part consists of burning the fuel in the car (tank to wheel). The suggested well to wheel process for an ICE based vehicle can be summarized by Fig. 7.1.
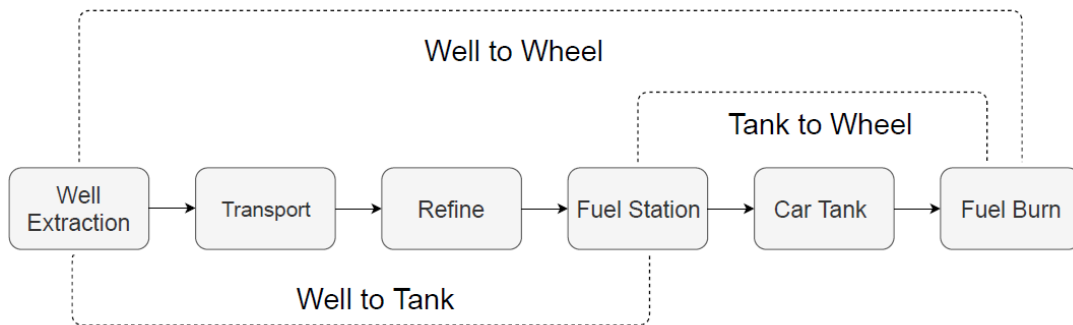
Figure 7.1 Well to wheel of an ICEV

The greenhouse gas (GHG) emissions can be calculated from [41] by the following equation:

$$GHG_{WtW-ICE} = \left(GHG_{WtT_o} + GHG_{TtW_o}\right)\eta_{ICE} \qquad (7.1)$$

$$o = [Diesel, gasoline]$$

$GHG_{WtW-ICE}$ represents the total GHGs resulting from an ICEV; it is expressed in gCO_2/Km. GHG_{WtT_o} represents the total GHGs emitted during the well to tank process, i.e the GHG_{WtT_o} would account for all CO_2 emitted from the oil extraction up till it reaches the fuel station. Similarly, the term GHG_{TtW_o} would account for all CO_2 emitted from the burning of fuel in the internal combustion engine (tail pipe emissions). Both GHG_{WtT_o} and GHG_{TtW_o} are expressed in gCO_2/liter. The η_{ICE} represents the efficiency of the ICE and is given in liter/km. Table 7.1 shows the average CO2 emissions for a subcompact car when the fuel type is gasoline or diesel.

Table 7.1 Internal Combustion Engine CO$_2$ Emissions for a Subcompact Car [40]

Vehicle category	Fuel type	Well-to-tank (g CO2/km)	Tank-to-wheel (g CO2/km)	Well-to-wheel (g CO2/km)
Subcompact	Gasoline	84.5	16.9	101.4
	Diesel	74.2	15.6	89.8

B. WTW for an FCHEV-CD

For a fuel cell hybrid electric vehicle operating in a charge depletion strategy, the WTW can be divided into two main parts: the first part is mining for the primary energy source and transporting it to the power generation utilities, and the second part consists of charging the electric battery driving the electric car. The first part is called well to power plant and the second part is be called power plant to wheel. Fig. 7.2 summarizes the complete well to wheel analysis for an FCHEV in charge depletion (CD) mode.
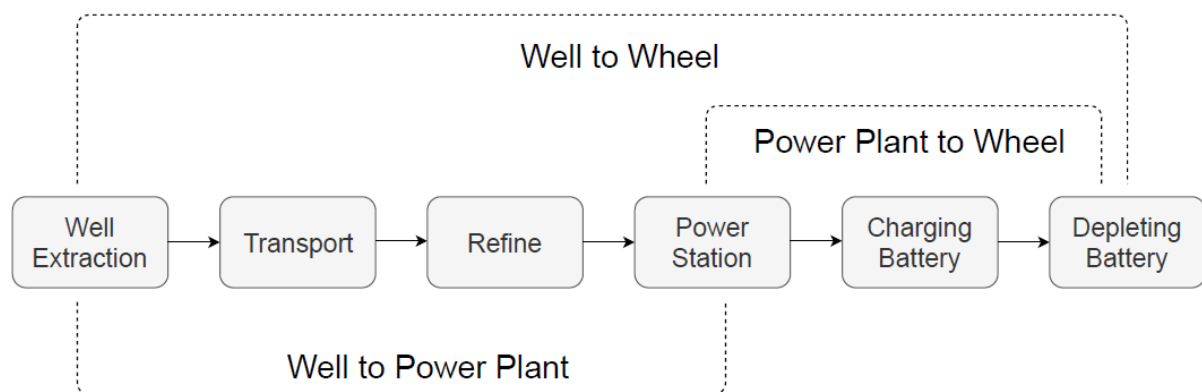
Figure 7.2 Well to wheel path for a battery electric vehicle

The total GHGs produced from an electric vehicle or a FHECV being operated in CD mode is given by (7.2). Note that this type of vehicles has zero tail pipe emissions. G_{WtW-CD} represents the equivalent amount of gCO_2/km. GHG_{WtP_e} and GHG_{PtW_e} are expressed in gCO_2/kWh and η_{CD} is expressed in kWh/km.

$$G_{WtW-CD} = \left[\sum_e \mu_{e,c} \left(G_{WtP_e} + G_{PtW_e}\right)\right] \eta_{CD} \tag{7.2}$$

$c = [US, UK, China \dots]$
$e = [Coal, Gas, Nuclear, Solar, Wind, Hydro]$

Table 7.2 CO$_2$ Emissions From Electricity Generation Mix [42,43]

Technology	Min	Max	Mean
	Emissions g/kWh		
Coal	756	1310	1033
Oil	547	935	741
Gas	362	891	626.5
Biofuels	10	101	55.5
Waste	168	1000	584
Nuclear	2	130	66
Hydro	2	237	119.5
Geothermal	39	78	58.5
Solar_PV	9.4	300	154.7
Solar_Thermal	30	150	90
Wind	6	124	65
Tidal	10	20	15

The CO$_2$ emissions for electricity generation using different technologies is shown is table 7.2. Coal and oil have the highest emissions among the different technologies listed. The electricity generation mix of each country ($\mu_{e,c}$) can be found in Appendix B.

The last parameter that is still needed to be found in order to calculate the total CO$_2$ emissions for the electric vehicle is η_{CD}. Recall that the η_{CD} is defined as the number of kWh required to move the FCHEV per km. This number is obtained by simulating our FCHEV in the charge depletion strategy, i.e using zero energy from the fuel cell. The battery

SOC over the two drive cycles is shown in Fig. 7.3 . The corresponding η_{CD} is then calculated and the results are shown in Table 7.3.
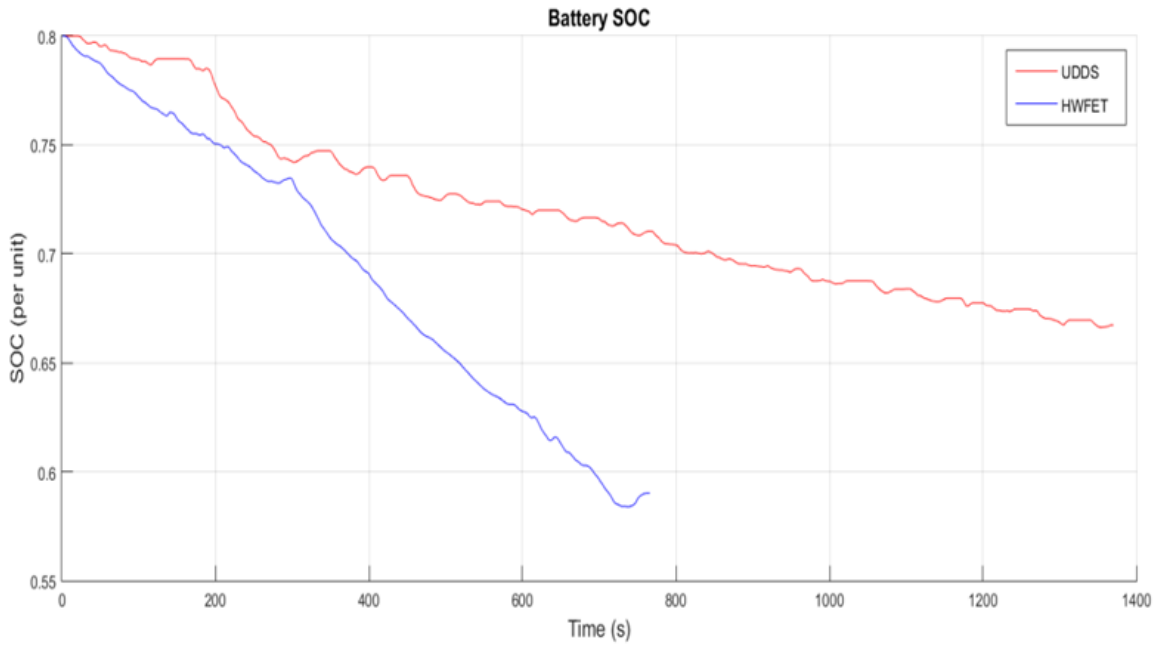
Figure 7.3 Battery SOC on UDDS and HWFET Cycles

Table 7.3 FCHEV-CD Efficiency (η_{CD})

Drive Cycle	Distance Travelled in Trip (km)	Energy Supplied By Battery (kWh)	η_{CD} (kWh/km)
HWFET	16.51	2.09	0.13
UDDS	12	1.34	0.12

C. WTW for an FCHEV in CS mode

The well to wheel analysis for a fuel cell hybrid electric vehicle in the charge sustaining mode follows a similar path to that of an internal combustion engine. The main difference lies in the type of fuel which is hydrogen in the case of an FCHEV having a Proton-exchange membrane fuel cell. G_{WtW-CS} accounts for all CO_2 emitted from extracting the production of hydrogen till hydrogen fuel stations (FCHEVs have zero tail pipe emissions). G_{WtW-CS} is expressed in gCO_2/Km. GHG_{WtP_h} and GHG_{PtW_h} are expressed in gCO_2/gH_2 and η_{CS} is expressed in gH_2/Km.

$$G_{WtW-CS} = \left[\sum_h \mu_h * \left(GHG_{WtP_h} + GHG_{PtW_h} \right) \right] * \eta_{CS} \qquad (7.3)$$

$h = [Steam\ methane, electrolysis, biomass]$

Table 7.4 shows the CO_2 emissions per grams of kW_{H2} for various production methods.

Table 7.4 CO2 Emissions from H2 Production [44]

	Technology	Emissions ($kgCO_2/kgH_2$)
Hard Coil	With CCUS, 90 % capture rate	2.5
	Without CCUS	20
Natural Gas	With CCUS, 90 % capture rate	1.5
	With CCUS, 56 % capture rate	4.5
	Without CCUS	8.5
Electricity	Renewable or nuclear	0.8
	Gas-fired Generation	17.5
	Coal-fired generation	39.5
	World average electricity mix	26.2

η_{CS} in (7.3) is calculated in a similar manner to η_{CD} . The FCHEV is simulated over the UDDS and on the HWFET cycle. The simulation is done in a charge sustaining mode and zero energy is supplied from the battery. The fuel cell energy on both cycles is shown in Fig. 7.4. The value for η_{CS} is calculated and shown in table 7.5.
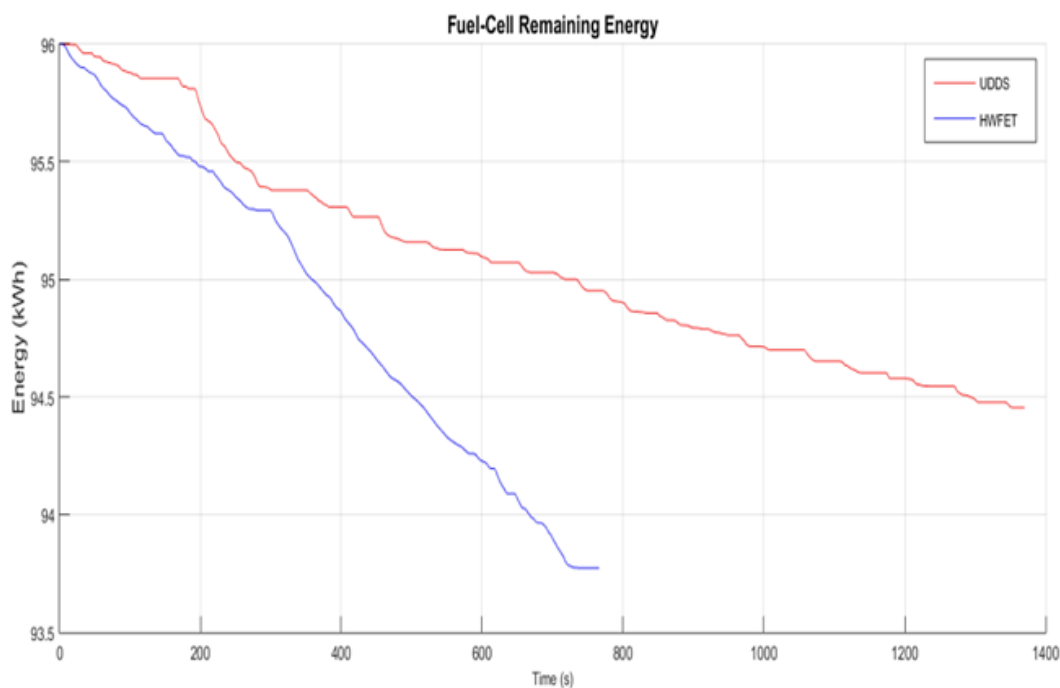
Figure 7.4 Fuel-Cell Reamining energy on UDDS and HWFET cycles

50

Table 7.5 FCHEV-CS Efficiency (η_{CS})

Drive Cycle	Distance Travelled in Trip (km)	Hydrogen Consumed (g)	η_{CS} (g H$_2$/Km)
HWFET	16.51	128.4	7.8
UDDS	11.99	80.7	6.7

D. Results

The emissions resulting from our previous advanced design in Chapter 6 will be calculated and compared against an ICE based car, belonging to the same class (subcompact car). The average emission for an ICE based subcompact car is already shown in table 7.1. The emissions from our FCHEV-CD design are calculated in 7 regions of the world. These regions include Africa, Asia and Pacific, Central America, Europe, Latin and North America. The selection of the countries in each region is based on having different generation mixes as well single source of electricity generation. The results of CO_2 emissions are shown for each region from table 7.6 to table 7.12. Each table shows the CO_2 emissions by country, a minimum and maximum value, and their corresponding mean. Some FCHEV emissions are marked in red because they represent a very high amount of CO_2 that is equal to exceeds those of a gasoline or diesel ICE car (Table 7.1). Looking at these tables and taking the low calculated value, it looks like an FCHEV-CD design would emit less CO_2 in almost all countries except for Mongolia (85.8 gCO_2 / km) where emissions are high but still less than the average ICE car whether that car is operated on gasoline (101.4 gCO_2 / km) or diesel fuel (89.8 gCO_2 / km). Both CO_2 emissions from an EV used in these two countries would still be less than values in table 7.1.

If we take the maximum value of emissions, we notice that most countries would report negative for the integration of an FCHEV-CD. This is clear as the emissions in most of the countries would be higher than corresponding ICE based subcompact car. In this case the FCHEV should not be used in CD mode as it would lose its environmental value and can be even more polluting than a traditional car. However, despite taking the maximum value for

EV emissions, countries having an energy generation mix based on renewable energy sources would still benefit from using a FCHEV in CD mode. FCHEVs-CD in countries such as France, Iceland, Sweden, Uruguay and Canada would still have way less emissions than an ICE based vehicle, even when maximum CD emissions are compared to average ICE emissions.

Now if we compare mean value of CO_2 from FCHEV-CD design to mean values of ICE emissions, we see FCHEVs would poorly reduce CO_2 emissions in countries having a large share of coal/oil in their generation mix. In fact, FCHEVs in Indonesia, Australia, China, Mongolia and Poland would be more polluting than diesel cars. Moreover, countries such as Lebanon and Greece would slightly benefit from EVs integration.

Lastly, if we compare the emissions of the FCHEV-CS with respect to the FCHEV-CD and ICE, we see that the CO_2 emissions associated with FCHEV-CS design are still high. The emissions associated with an FCHEV are directly related to source of fuel and the efficiency of the fuel cell. From table 7.13, we see that if hard coil is used without Carbon, capture utilization and storage (CCUS) emissions would reach 144.2 g CO_2/km; however with CCUS 90 % capture rate emissions are reduced to 18 gCO_2/km. If natural gas is used without CCUS, the emissions from an FCHEV-CS are 61.3 gCO_2/km if CCUS is used with % capture rate emissions are reduced to only 10.8 gCO_2/km. Finally, if electrolysis is used to produce the hydrogen, the emissions would be directly related to the electricity generation mix. If we take the world average generation mix, the emissions for an FCHEV-CS are remarkably high reaching 188.9 gCO_2/km. The emissions for an FCHEV-CS are at its highest if the source of electricity is from coal-fired generation (284.8 gCO_2/km). This number gets better if gas-fired generation is used instead. In case a 100 percent renewable or nuclear energy source is used for electrolysis then emissions are almost negligible (5.8 gCO_2/km).

Table 7.6 CO$_2$ Emissions for FCHEV-CD in Africa

Country	Low (g CO$_2$/km)	Max (g CO$_2$/km)	Mean (g CO$_2$/km)
Algeria	43.3	106	74.6
Ghana	28.6	73.7	51.2
Kenya	15.6	37	26.3
Nigeria	35.4	92.1	63.7
Senegal	58.5	103	80.7
South Africa	80.9	142	111.4
Tunisia	41.9	103.6	72.7

Red colored emissions indicate FCHEV emissions are around or greater than that of an ICE based vehicle.

Table 7.7 CO$_2$ Emissions for FCHEV-CD in Asia and Pacific

Country	Low (g CO$_2$/km)	Max (g CO$_2$/km)	Mean (g CO$_2$/km)
Australia	67.3	126	96.7
China	62.9	116.9	89.9
Indonesia	64.7	122.7	93.7
Japan	53.1	110.1	81.6
Korea	20.8	57	38.9
Malaysia	58.3	117.7	88
Mongolia	85.8	149.3	117.5
New Zealand	9.1	37.8	23.4
Pakistan	34.2	77.7	55.9
Philippines	57.1	109	83

Table 7.8 CO$_2$ Emissions for FCHEV-CD in Central America

Country	Low (g CO$_2$/km)	Max (g CO$_2$/km)	Mean (g CO$_2$/km)
Costa Rica	2	25.7	13.9
Nicaragua	32.2	61.1	46.6
Panama	23.5	58	40.7

Table 7.9 CO2 Emissions for FCHEV-CD in Europe

Country	Low (g CO$_2$/km)	Max (g CO$_2$/km)	Mean (g CO$_2$/km)
Belarus	43	105.3	74.2
Bolivia	34.2	88.7	61.5
France	5.2	26.9	16.1
Germany	44.8	90.7	67.7
Greece	50	101.9	75.9
Iceland	1.4	23	12.2
Italy	34.2	82.6	58.4
Moldova	41.4	102.9	72.2
Poland	75	133.5	104.2
Portugal	29.9	70.7	50.3
Russia	35.5	84.3	59.9
Spain	24.9	60.4	42.7
Sweden	1.8	24.1	12.9
United Kingdom	27.6	70.2	48.9

Table 7.10 CO$_2$ Emissions for FCHEV-CD in Latin America

Country	Low (g CO$_2$/km)	Max (g CO$_2$/km)	Mean (g CO$_2$/km)
Argentina	33	81.2	57.1
Brazil	10.3	41.3	25.8
Chile	43.4	90.3	66.8
Colombia	19.9	58.8	39.3
Mexico	42.7	96.4	69.5
Uruguay	2.6	25.8	14.2
Venezuela	20.9	60.2	40.5

Table 7.11 CO$_2$ Emissions for FCHEV-CD in Middle East

Country	Low (g CO$_2$/km)	Max (g CO$_2$/km)	Mean (g CO$_2$/km)
Bahrain	43.2	106.2	74.7
Egypt	44	100.8	72.4
Jordan	43.6	103	73.3
Kuwait	57.2	109.6	83.4
Lebanon	63.9	109.8	86.8
Oman	43.7	106.3	75
Saudi Arabia	52.1	108.3	80.2
Turkey	45.1	96.2	70.6

Table 7.12 CO$_2$ Emissions for EV in North America

Country	Low (g CO$_2$/km)	Max (g CO$_2$/km)	Mean (g CO$_2$/km)
Canada	13.4	45.6	29.5
United States	43.2	91.7	67.5

Table 7.13 CO$_2$ Emissions for FCHEV-CS

	Technology	Emissions (gCO$_2$/km)
Hard Coil	With CCUS, 90 % capture rate	18
	Without CCUS	144.2
Natural Gas	With CCUS, 90 % capture rate	10.8
	With CCUS, 56 % capture rate	32.5
	Without CCUS	61.3
Electricity	Renewable or nuclear	5.8
	Gas-fired Generation	126.2
	Coal-fired generation	284.8
	World average electricity mix	188.9

54

CHAPTER VIII

CONCLUSION

This thesis has presented an optimal design for fuel cell hybrid electric vehicles. The methodology is based on Ordinal Optimization (OO) that requires a simulation of the car operation that was done using dynamic programming. To speed up the process of car simulation, a single stage DP (SSDP) was used in the simple model instead, and a Two-Step SSDP was used in the accurate model. To increase the accuracy of the model, electric losses in the power train are included. These losses account for motor, switching, conduction and reverse recovery losses. The effect of using light weight material in the design of FCHEVs is also studied. For this purpose, we designed two FCHEV: one that served as a baseline model and the other as the advanced one. The baseline model had a traditional body made mainly from steel, while the advanced one had a light body made from different light materials. Remarkable savings in hydrogen consumption and in components sizing are obtained. The advanced design had a 40 kW fuel cell, a 5 kg H_2 tank, 3 kWh battery and 100 kW motor size. On the other hand the baseline had a 60 kW fuel cell, a 6 kg H_2 tank a 4 kWh battery and a 140 kW motor. Thus the advanced design had a 1 kg smaller H2 tank, a 20 kW smaller fuel cell size and 1 kWh smaller battery size. Moreover, the advanced design had remarkable savings hydrogen consumption. On the UDDS drive cycle, 23 % of H_2 savings are obtained and on the HWFET H_2 savings reached 15.1%. The total annualized cost for the advanced design is \$ 6926 while that of the baseline is \$ 8071; this reduces the yearly costs by 14.2 %. Lastly, an environmental analysis was performed to quantify the amount of CO_2 released from different designs. The electricity generation mix of different countries was used. The amount of CO_2 emissions resulting from an FCHEV being operated in the charge depletion mode were compared to FCHEV in the charge sustaining mode and to subcompact ICE based vehicles. The amount of emissions per design varied greatly depending on the primary source

of energy. In some countries emissions from an FCHEV in CD mode can reach 144 gCO_2 / km. On the other hand an FCHEV in CS mode releases 284.8 gCO_2 / km if coal-fired plants are used. In both cases if renewable energy sources are used the emissions for both modes are significantly lowered.

For future work, further simplifications in the simple model can be achieved. This can be done by extra simplifications in the drive cycles and by utilizing a lower number of fuel cell levels. Moreover, the same work can be applied to public transportation means such as buses. In fact, it would be very interesting to calculate the remarkable savings in terms of emissions and costs per passenger if the tools developed in this thesis are applied for example to a fuel cell bus.

Appendix A

Nomenclature

α	Annuity factor
γ_{BT}	Battery cost parameter in \$/ kWh
δ	Inclination angle
Δt	Time step duration between stage k and k-1
$\varphi_F(F_k)$	Cost rate of operating the fuel cell at F_k in \$/h
$\varphi_B(B_k)$	Internal energy rate of battery at B_k (kW)
ρ	Density of the air
B_k	Battery power at stage k (kW)
B^{max}	Size for the battery power (kW)
D_k	Power demand at stage k (kW)
F_k	Fuel cell power at stage k (kW)
F^{max}	Size of the fuel cell (kW)
H_2^{max}	Size for the hydrogen tank (kg)
R_k	Brake power (kW) at stage k
$I_C(n)$	Investment cost of design n
J	Design cost function
K	Number of time steps in drive cycle
M_k	Motor power (kW)
M^{max}	Motor power rating (kW)
$O_C(n)$	Operational cost of design n
R_F	Fuel cell ramp up and down limits (kW/h)
R_B	Battery ramp up and down limits (kW/h)

Acronyms

Abbreviation	Full Term
LIB	Lithium Ion Battery
LAB	Lead Acid Battery
F_{ad}	Aerodynamic drag force
F_{rr}	Rolling resistance force
F_{hc}	Hill climbing force
F_{la}	Acceleration force
MPGGE	Miles per gallons gas equivalent

Appendix B

Table B.1 Electricity Generation Mix in Africa

Country	Coal	Oil	Gas	Biofuels	Waste	Nuclear	Hydro	Geothermal	Solar PV	Wind
Algeria	0	1.4	98.2	0	0	0	0.3	0	0.1	0
Ghana	0	17.6	39.5	0	0	0	42.7	0	0.2	0
Kenya	0	20.7	0	1.3	0	0	34.3	43.1	0	0.6
Nigeria	0	0	81.9	0	0	0	18.1	0	0	0
Senegal	0	88.5	1.7	1.4	0	0	8.2	0	0.1	0
South Africa	89.6	0.1	0	0.1	0	5.9	1.6	0	1	1.5
Tunisia	0	0.2	96.8	0	0	0	0.2	0	0.3	2.4

Table B.2 Electricity Generation Mix in Asia and Pacific

Country	Coal	Oil	Gas	Biofuels	Waste	Nuclear	Hydro	Geothermal	Solar PV	Wind
Australia	63.6	2.2	19.6	1.5	0	0	6	0	2.4	4.8
China	68.2	0.2	2.7	1	0.2	3.4	19.2	0	1.2	3.8
Indonesia	54.4	6.3	26.4	0.7	0	0	7.8	4.3	0	0
Japan	33.7	8.2	39.2	1.4	1.8	1.7	8.2	0.2	4.9	0.6
Korea	18.8	5.6	0	0	0	0	75.6	0	0	0
Malaysia	44.1	0.8	41.6	0.5	0	0	12.8	0	0.2	0
Mongolia	92.7	3.4	0	0	0	0	1	0	0.1	2.7
New Zealand	2.5	0	13.5	1.4	0	0	59.9	17.3	0.1	5.4
Pakistan	0.1	32.8	29.2	0.5	0	4.3	32.1	0	0.2	0.7
Philippines	47.7	6.2	21.9	0.8	0	0	8.9	12.2	1.2	1.1

Table B.3 Electricity Generation Mix in Central America

Country	Coal	Oil	Gas	Biofuels	Waste	Nuclear	Hydro	Geothermal	Solar PV	Wind
Costa Rica	0	1.8	0	1.6	0	0	73.8	12.3	0	10.5
Nicaragua	0	47.8	0	11.6	0	0	9.3	15.4	0	15.9
Panama	6.1	27.3	0	0.3	0	0	59.9	0	0.7	5.7

Table B.4 Electricity Generation Mix in Europe

Country	Coal	Oil	Gas	Biofuels	Waste	Nuclear	Hydro	Geothermal	Solar PV	Wind
Belarus	0.1	1.7	96.9	0.4	0.1	0	0.4	0	0.1	0.2
France	1.9	0.5	6.3	0.9	0.8	72.6	11.7	0	1.5	3.9
Germany	42.2	0.9	12.7	7	2	13.1	4	0	5.9	12.1
Greece	34.7	10.2	27.3	0.5	0.4	0	10.2	0	7.2	9.5
Iceland	0	0	0	0	0	0	72.6	27.3	0	0
Italy	13.3	4.2	43.6	5.9	1.7	0	15.3	2.2	7.6	6.1
Moldova	0	0.3	95.5	0.2	0	0	3.9	0	0	0.1
Poland	79.8	1.4	4.7	4.8	0.1	0	1.6	0	0.1	7.6
Portugal	21	2.2	20.9	4.6	1	0	28.1	0.3	1.4	20.7
Russia	15.7	1	47.8	0	0.2	18	17.1	0	0	0
Spain	13.6	6.2	19.2	1.8	0.5	21.3	14.5	0	2.9	17.8
Sweden	0.7	0.3	0.4	6.3	2.1	40.4	39.8	0	0.1	9.9
United Kingdom	9.3	0.5	42.2	8	2.2	21.1	2.5	0	3.1	11

Table B.5 Electricity Generation Mix in Middle East

Country	Coal	Oil	Gas	Biofuels	Waste	Nuclear	Hydro	Geothermal	Solar PV	Wind
Bahrain	0	0	100	0	0	0	0	0	0	0
Egypt	0	19.7	72.2	0	0	0	6.9	0	0.1	1.1
Jordan	0	11	84.3	0	0	0	0.2	0	2.5	2
Kuwait	0	63.9	36.1	0	0	0	0	0	0	0
Lebanon	0	98	0	0	0	0	2	0	0	0
Oman	0	2.7	97.3	0	0	0	0	0	0	0
Saudi Arabia	0	40.6	59.4	0	0	0	0	0	0	0
Turkey	33.7	0.7	32.6	0.6	0	0	24.6	1.8	0.4	5.7

Table B.6 Electricity generation mix in Latin America

Country	Coal	Oil	Gas	Biofuels	Waste	Nuclear	Hydro	Geothermal	Solar PV	Wind
Argentina	1.7	14.2	51.2	1.2	0	5.6	25.7	0	0	0.4
Brazil	4.5	2.6	9.8	8.8	0	2.7	65.8	0	0	5.8
Chile	38.1	3.7	14.9	7.5	0	0	29.3	0	3.3	3.1
Mexico	10.8	10.6	60	0.5	0	3.3	9.6	1.9	0.1	3.2
Uruguay	0	3.3	0	13.7	0	0	59.2	0	1.1	22.6
Venezuela	0	15.9	24	0	0	0	60.1	0	0	0

Table B.7 Electricity Generation mix in North America

Country	Coal	Oil	Gas	Biofuels	Waste	Nuclear	Hydro	Geothermal	Solar PV	Wind
Canada	9.3	1.2	9.3	1.9	0	15.2	58	0	0.5	4.6
United States	31.4	0.8	32.9	1.4	0.4	19.5	6.8	0.4	1.1	5.3

Table B.8 Emissions From the Upstream Portion of Natural Gas to Hydrogen Value Chain

Reference	Spath and Mann	Miller et al.	Ramsden et	Edwards et al (2014)	
Emissions (mg/kWhH2)	No CCS, gas transport included	No CCS, gas transport included	No CCS, gas transport included	No CCS, gas transport excluded	With CCS, gas transport excluded
CO_2	39,889	21,020	17,429	7338	7617
CH_4	1681	710	1591	403	418
N2O	0.38	4	0.29	0	0
VOC	-	31	-	-	-
CO	154	101	-	-	-
NOx	282	129	-	-	-

Table B.9 Emissions from the Production of Biomass Feedstock Used in the Production of Hydrogen Via Gasification

Emission	Emissions from biomass feedstock (g/kWhH2)
CO_2 (fossil only)	15.4
CH_4	0.030
N2O	0.046
VOC	0.015
CO	0.033
NO_x	0.082
PM_{10}	0.0061
$PM_{2.5}$	0.0030

Table B.10 GHG Emissions From Coal Production

Species	Emissions (g/kWhH2)		
	With CCS (Ramsden et al., 2013)	With CCS (Edwards et al., 2014)	Without CCS (Edwards et al.,2014)
CO_2	3.2	44	38
CH_4	0.54	2.9	2.5
N_2O	0.0001	0.0018	0.0015

Table B.11 Emissions from the Production of Hydrogen from Wind-Generated Electricity, Covering the Production of Electricity (Including Construction and Operation of Wind Turbines)

Emission	Emissions from wind turbine (mg/kWh H2)	Emissions from electrolysis mg/kWh H2
CO_2	18,829	1,061
CO	18.3	0.80
CH_4	7.0	0.21
NO_x	54.7	56.2
Nitrous oxide	0.85	0.071
NMHC	69.8	8.2
Particulates	686	5.1
SOx	95.7	40.4

Table B.12 Emissions From the Production of Electricity used in Electrolysis (uses USA grid) (Miller et al., 2017)

Emission (mg/kWh)	Solar electrolysis (centralised)		USA grid electricity (distributed)	
	Gaseous hydrogen	Liquid hydrogen	Gaseous hydrogen	Liquid hydrogen
CO_2	72346	217468	817931	1020106
CH_4	158	469	1775	2214
N_2O	3	6.1	18	21
VOC	9.1	30	113	140
CO	45.7	143.1	533	664
NO_x	113	344	1267	1577
PM_{10}	18	52	201	250
$PM_{2.5}$	12	33	122	152
SO_x	158	475	1800	2244

REFERENCES

[1] "Climate change and health," World Health Organization. [Online]. Available: http://www.who.int/news-room/fact-sheets/detail/climate-change-and-health. [Accessed: 27-Jun-2018].

[2] "Sources of Greenhouse Gas Emissions | US EPA", US EPA, 2018. [Online]. Available: https://www.epa.gov/ghgemissions/sources-greenhouse-gas-emissions. [Accessed: 28- Jun- 2018].

[3] A. Khajepour et al, Electric and Hybrid Vehicles: Technologies, Modeling and Control - A Mechatronic Approach. 2014.

[4] M. Ehsani et al, Modern Electric, Hybrid Electric, and Fuel Cell Vehicles: Fundamentals, Theory, and Design. (2nd ed.) 2010;

[5] S. Onori, G. Rizzoni and L. Serrao, Hybrid Electric Vehicles : Energy Management Strategies. (1st 2016 ed.) 2015;2016;. DOI: 10.1007/978-1-4471-6781-5

[6] J. Larminie and J. Lowry, Electric Vehicle Technology Explained. Chichester: Wiley, 2003.

[7] J. Y. Yong et al, "A review on the state-of-the-art technologies of electric vehicle, its impacts and prospects," Renewable and Sustainable Energy Reviews, vol. 49, pp. 365-385, 2015.

[8] The History of the Electric Car", Energy.gov, 2018. [Online]. Available: https://www.energy.gov/articles/history-electric-car. [Accessed: 01- Jul- 2018].

[9] R. M. Dell, P. T. Moseley and D. A. J. Rand, Towards Sustainable Road Transport. (1st ed.) 2014;2013.

[10] W. Enang and C. Bannister, "Modelling and control of hybrid electric vehicles (A comprehensive review)," Renewable and Sustainable Energy Reviews, vol. 74, pp. 1210-1239, 2017

[11] M. Ehsani, Y. Gao and J. M. Miller, "Hybrid Electric Vehicles: Architecture and Motor Drives," Proceedings of the IEEE, vol. 95, (4), pp. 719-728, 2007.

[12] H. S. Das, C. W. Tan and A. H. M. Yatim, "Fuel cell hybrid electric vehicles: A review on power conditioning units and topologies," Renewable and Sustainable Energy Reviews, vol. 76, pp. 268-291, 2017.

[13] O. Z. Sharaf and M. F. Orhan, "An overview of fuel cell technology: Fundamentals and applications," Renewable and Sustainable Energy Reviews, vol. 32, pp. 810-853, 2014.

[14] S. Mekhilef, R. Saidur and A. Safari, "Comparative study of different fuel cell technologies," Renewable and Sustainable Energy Reviews, vol. 16, (1), pp. 981-989, 2012.

[15] L. B. Braga et al, "Comparative analysis between a PEM fuel cell and an internal combustion engine driving an electricity generator: Technical, economical and ecological aspects," Applied Thermal Engineering, vol. 63, (1), pp. 354-361, 2014.

[16] A. F. Burke, "Batteries and Ultracapacitors for Electric, Hybrid, and Fuel Cell Vehicles,"Proceedings of the IEEE, vol. 95, (4), pp. 806-820, 2007.

[17] A. Khaligh and Z. Li, "Battery, Ultracapacitor, Fuel Cell, and Hybrid Energy Storage Systems for Electric, Hybrid Electric, Fuel Cell, and Plug-In Hybrid Electric Vehicles: State of the Art," IEEE Transactions on Vehicular Technology, vol. 59, (6), pp. 2806-2814, 2010.

[18] M. Redelbach, E. D. Özdemir and H. E. Friedrich, "Optimizing battery sizes of plug-in hybrid and extended range electric vehicles for different user types," Energy Policy, vol. 73, pp. 158-168, 2014.

[19] C. Sinkaram, V. S. Asirvadam and N. Bin Mohd Nor, "Capacity study of lithium ion battery for hybrid electrical vehicle (HEV) a simulation approach," in 2013, . DOI: 10.1109/ICSIPA.2013.6707987.

[20] G. Ren, G. Ma and N. Cong, "Review of electrical energy storage system for vehicular applications," Renewable and Sustainable Energy Reviews, vol. 41, pp. 225-236, 2015.

[21] J. Haase et al, "Analysis of batteries in the built environment an overview on types and applications," in 2017, DOI: 10.1109/IECON.2017.8217424

[22] S. P. Kodali and S. Das, "Implementation of five level charging scheme in lithium ion batteries for enabling fast charging in plug-in hybrid electric vehicles," in 2017, . DOI: 10.1109/NPEC.2017.8310450

[23] J. Li et al, "Toward Low-Cost, High-Energy Density, and High-Power Density Lithium-Ion Batteries," Jom, vol. 69, (9), pp. 1484-1496, 2017.

[24] K. K. Yeung et al, "Enhanced cycle life of lead-acid battery using graphene as a sulfation suppression additive in negative active material," RSC Advances, vol. 5, (87), pp. 71314-71321, 2015.

[25] N. Sugumaran, P. Everill, S. Swogger and D. Dubey, "Lead acid battery performance and cycle life increased through addition of discrete carbon nanotubes to both electrodes", Journal of Power Sources, vol. 279, pp. 281-293, 2015.

[26] S. F. Tie and C. W. Tan, "A review of energy sources and energy management system in electric vehicles," Renewable and Sustainable Energy Reviews, vol. 20, pp. 82-102, 2013.

[27] R. Zhang and J. Tao, "GA based fuzzy energy management system for FC/SC powered HEV considering H2 consumption and load variation," IEEE Transactions on Fuzzy Systems, pp. 1-1, 2017.

[28] L. Jin et al, "Research on the control strategy optimization for energy management system of hybrid electric vehicle," in 2017, . DOI: 10.1109/ICRAE.2017.8291393.

[29] S. H. Karaki et al, "Fuel Cell Hybrid Electric Vehicle Sizing using Ordinal Optimization,"SAE International Journal of Passenger Cars - Electronic and Electrical Systems, vol. 8, (1), pp. 60-69, 2015.

[30] A. Rezaei et al, "A New Real-Time Optimal Energy Management Strategy for Parallel Hybrid Electric Vehicles," IEEE Transactions on Control Systems Technology, pp. 1-8, 2017.

[31] L.Guo et al,"A fast algorithm for nonlinear model predictive control applied to HEV energy management systems, vol. 60, (9), pp. 190-206, 2017.

[32] J. Larminie and J. Lowry, Electric Vehicle Technology Explained. Chichester: Wiley, 2003.

[33] Y. Ho et al, Ordinal Optimization: Soft Optimization for Hard Problems. New York: Springer, 2007.

[34] S. S. Williamson, A. Emadi and K. Rajashekara, "Comprehensive Efficiency Modeling of Electric Traction Motor Drives for Hybrid Electric Vehicle Propulsion Applications," IEEE Transactions on Vehicular Technology, vol. 56, (4), pp. 1561-1572, 2007.

[35] Energy.gov. (2019). [online] Available at:https://www.energy.gov/sites/prod/files/2014/04/f15/10097517.pdf [Accessed 29 Jul. 2019].

[36] R. B. Sepe, "Quasi-behavioral model of a voltage fed inverter suitable for controller development," *Proceedings of 1995 IEEE Applied Power Electronics Conference and Exposition - APEC'95*, Dallas, TX, USA, 1995, pp. 176-182 vol.1. doi: 10.1109/APEC.1995.469017

[37] J. M. Miller, Propulsion Systems for Hybrid Vehicles. Stevenage: The Institution of Engineering and Technology, 2010;2011;7.

[38] P. K. Mallick, Materials, Design and Manufacturing for Lightweight Vehicles. 2010.

[39] J. HIRSCH, "Recent development in aluminium for automotive applications," Transactions of Nonferrous Metals Society of China, vol. 24, (7), pp. 1995-2002, 2014.

[40] Lotus Engineering Inc. 2010. "An Assessment Of Mass Reduction Opportunities For A 2017 – 2020 Model Year VehicleProgram".https://www.theicct.org/sites/default/files/publications/Mass_reduction_final_2010.pdf

[41] J. Woo, H. Choi and J. Ahn, "Well-to-wheel analysis of greenhouse gas emissions for electric vehicles based on electricity generation mix: A global perspective," Transportation Research Part D, vol. 51, pp. 340-350, 2017.

[42] Comparison of Lifecycle Greenhouse Gas Emissions of of Various Electricity Generation Sources. http://www.worldnuclear.org/uploadedFiles/org/WNA/Publications/Working_Group_Reports/comparison_of_lifecycle.pdf. Accessed 13 Jul 2019

[43] N. Y. Amponsah et al, "Greenhouse gas emissions from renewable energy sources: A review of lifecycle considerations," Renewable and Sustainable Energy Reviews, vol. 39, pp. 461-475, 2014.

[44] Energy.gov. (2019). [online] Available at: https://www.energy.gov/sites/prod/files/2014/04/f15/10097517.pdf [Accessed 31 Jul. 2019].